

UNCLASSIFIED

AD 297 460

*Reproduced
by the*

**ARMED SERVICES TECHNICAL INFORMATION AGENCY
ARLINGTON HALL STATION
ARLINGTON 12, VIRGINIA**



UNCLASSIFIED

NOTICE: When government or other drawings, specifications or other data are used for any purpose other than in connection with a definitely related government procurement operation, the U. S. Government thereby incurs no responsibility, nor any obligation whatsoever; and the fact that the Government may have formulated, furnished, or in any way supplied the said drawings, specifications, or other data is not to be regarded by implication or otherwise as in any manner licensing the holder or any other person or corporation, or conveying any rights or permission to manufacture, use or sell any patented invention that may in any way be related thereto.

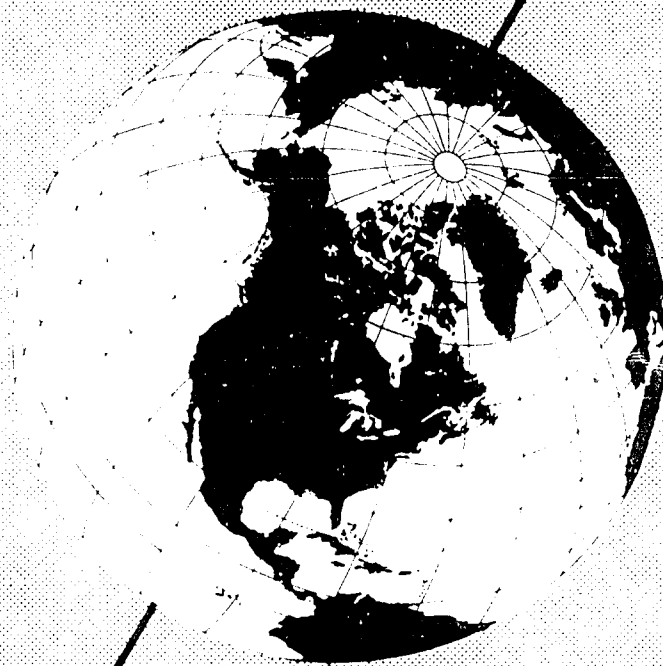
63-2-2

Research Report 73

SEPTEMBER, 1962

297 460

Scale Model Studies on Snow Drifting



Best Available Copy



U. S. ARMY
SNOW ICE AND PERMAFROST
RESEARCH ESTABLISHMENT
Corps of Engineers

ASTIA Availability Notice
Qualified requestors may obtain
copies of this report from ASTIA.

Research Report 73

SEPTEMBER, 1962

Scale Model Studies on Snow Drifting

by Gordon H. Strom, George R. Kelly,
Edwin L. Keitz, and Robert F. Weiss


U. S. ARMY SNOW ICE AND PERMAFROST
RESEARCH ESTABLISHMENT
Corps of Engineers

PREFACE

This report was prepared by the Research Division, College of Engineering, New York University, under Contract DA-11-190-ENG-31.

The research covered by this report was performed for USA SIPRE* under the general supervision of Dr. R. W. Gerdel, Chief, Environmental Research Branch.

This report has been reviewed and approved for publication by the Office of the Chief of Engineers, United States Army.


W. L. NUNGESSER
Colonel, Corps of Engineers
Director

Department of the Army Task 8X99-27-001-03

Manuscript received 8 January 1962

* Now a part of U. S. Army Cold Regions Research and Engineering Laboratory, 1 February 1962

CONTENTS

	Page
Preface	ii
Summary	vi
List of symbols	vii
Introduction	1
Theoretical analysis of saltation phenomena in snow drifting	2
Development of theory	2
Assumptions	2
Trajectory analysis	2
Particle - field interaction	5
Particle distribution	8
Correlation	9
Program for numerical solution	10
Numerical example	12
Summary of analysis of saltation phenomenon	15
Development of scale factors	15
Scale factors based on dimensional analysis	15
Scale factors based on theoretical analysis of saltation phenomena	21
Selection of model scale and snow simulator properties	24
Investigation and selection of material to be used as snow simulators in model experiments	26
Techniques and equipment	26
Measurement of free-fall velocity	26
Large drop chamber with still camera and strobalume	26
Two-camera technique	26
Drop chamber and high-speed motion picture camera	26
Density measurement	26
Weight and volume technique	27
Air suspension technique	27
Two-liquid technique	28
Free-fall velocity of snow particles	28
Physical properties of particulates to be used as snow simulators	28
Low-density materials	28
High-density materials	30
Free-fall velocity	30
Coefficient of restitution	32
Threshold velocity	32
Selection of a snow simulator from the materials tested	33
Wind tunnel modification	33
Scale model experiments on snow drifting characteristics of various structures	36
Clements-panel buildings oriented crosswind	36
Clements-panel buildings oriented downwind	40
Elevated radar type building	41
Snow fence models	41
Fuel storage tanks	41
Future work	42
References	50

CONTENTS (Cont'd.)

ILLUSTRATIONS

Figure		Page
1.	Forces and velocities of a particle -----	3
2.	Linear velocity profile assumed for boundary layer ----	3
3.	Assumed form of particle field at surface -----	6
4.	Maximum transverse angle of approach is shown to be 30° -----	6
5.	Interaction limitations -----	6
6.	Vector diagrams of particle velocity and velocity com- ponents before and after collision -----	7
7.	Definition of area for particle impaction used in eq 18 --	13
8.	Probability of scattering angle β_s -----	13
9.	Typical trajectory for glass sphere -----	14
10.	Probability of initial angle and velocity -----	14
11.	Particle distribution -----	15
12.	Drop chamber showing the Bell and Howell high-speed camera in position -----	27
13.	Terminal velocities of spherical particles of different density settling in air at 70F under the action of gravity -	27
14.	Relationship between particle diameter and particle density for cork -----	30
15.	Relationship between particle diameter and free-fall velocity for larger sized particles -----	30
16.	Relationship between particle diameter and free-fall velocity for all particles measured -----	33
17.	Relationship between particle density and fluid threshold velocity -----	33
18.	Relationship between particle diameter and fluid thresh- old velocity for cork -----	34
19.	Photomicrograph of 0.1 mm borax crystals -----	34
20.	Sketch of test section of New York University $3\frac{1}{2}$ x 7 ft wind tunnel -----	35
21.	Clements panel buildings nos. 2 and 3 oriented cross- wind, $\frac{1}{2}$ hr after start of test -----	37
22.	Clements panel buildings nos. 1, 2, and 3 oriented crosswind, 1 hr after start of test -----	37
23.	Side view of buildings nos. 1, 2, and 3 at the same time as shown in Figure 22 -----	38
24.	Clements panel buildings nos. 1, 2, and 3 oriented crosswind, 3 hr after start of test -----	38
25.	Clements panel buildings nos. 3 and 4 oriented cross- wind, 3 hr after start of test -----	39
26.	Clements panel buildings nos. 1, 2, and 3 oriented crosswind, $3\frac{1}{2}$ hr after start of test, $\frac{1}{2}$ hr after start of erosion -----	39
27.	Schematic view of drift pattern after 3 hr of snow deposition -----	40
28.	Clements panel buildings nos. 1, 2, and 3 oriented crosswind, 5 hr after start of tests, 2 hr after start of erosion -----	42
29.	Clements panel buildings oriented with the wind, 2 hr after start of test -----	43

CONTENTS (Cont'd.)
ILLUSTRATIONS (Cont'd.)

Figure		Page
30.	Clements panel buildings oriented with the wind, 2 hr after start of test -----	43
31.	Radar type building, 1 hr after start of test -----	44
32.	Radar type building, 1½ hr after start of test -----	44
33.	Schematic view of foundation used to support radar type building for test rerun -----	45
34.	Radar type building with special foundation, 2 hr after start of test -----	45
35.	Union Pacific type snow fence inclined 90°, 3 hr after start of test -----	46
36.	Union Pacific type snow fence inclined 60°, 2 hr after start of test -----	46
37.	Model of paper strip fence tested on the Greenland Ice Cap -----	47
38.	Paper strip fence, 3 hr after start of test -----	47
39.	V-shaped Union Pacific type fence prior to start of test -----	48
40.	Clear area downwind of V-shaped fence, after 2-hr test period -----	48
41.	Models representing 10-ft high fuel tanks, ½ hr after start of test -----	49
42.	Fuel tanks after 3 hr of blowing snow -----	49

TABLES

Table		Page
I.	Fall of 20 snow grains in 1/40 sec -----	29
II.	Physical properties of materials originally proposed as snow simulators -----	29
III.	Density tests on cork particles -----	31
IV.	Terminal velocity tests using high-speed motion picture -----	31

SUMMARY

Snow-drifting characteristics of various structures were studied by scale-model wind-tunnel experiments. Modeling criteria developed by two different methods were used as a basis for selecting a material for simulating snow in scale-model experiments and for determination of test variables.

A number of materials were tested for physical properties which would make them suitable for snow simulators. It was found that, for a 1/10 model scale, 0.01 cm diam crystalline borax was the best available material.

The work performed in the 3½ by 7 ft wind tunnel adequately demonstrated the feasibility of using geometrically and physically scaled synthetic snow in a wind tunnel. It was also shown that it is possible to present several years of arctic snowstorm environment in a few hours of wind-tunnel time. The actual tests showed these major points:

1. Close spacing of buildings will result in coalescence of drifts. This applies regardless of the orientation of the long axis of the building with respect to wind flow.
2. When rectangular buildings must be grouped in closely spaced units, it appears that they should be erected with the long axis parallel to the dominant wind direction. Channeling the wind flow between paired buildings oriented with the wind tends to keep the space between the longitudinal rows of buildings open.
3. Snow erosion may occur beneath buildings erected on columns above the surface. The columns must be carried to an unerodable stratum or they must be set on a crib foundation to prevent undermining of the footing.
4. A V-shaped snow fence produced a clear area downwind for a distance equal to approximately 25 times the height of the fence. This phenomenon may be applied to the protection of trench entrances to under-snow structures.
5. The tests with the borax snow simulator produced classic patterns of drifting very similar to those characteristic of cold dry arctic snow.
6. The drift patterns produced by the unidirectional flow in the tunnel probably were more concentrated longitudinally than those developed under natural conditions where some variation in wind direction and speed occurs during and following periods of blowing and drifting snow.

LIST OF SYMBOLS

A	defined after eq 8b
a_x	acceleration in x - direction
a_y	acceleration in y - direction
B	defined after eq 8b
b	perpendicular distance between particle centers
C	defined by eq 9
C_1, \dots, C_4	various constants explained where used
C_D	drag coefficient
C_f	surface friction coefficient
D_g	drag force
D_s	density scale factor
E	defined by eq 24b
e	coefficient of restitution for surface shear stress in boundary layer
F	general force on particle
$f(s)$	Laplace transform of $f(t)$
g	acceleration due to gravity
I_0	density of airborne particles
K	velocity profile scale factor
k_0, \dots, k_7	various constants explained where used
k_s	grain size of sand particles used in the original experiments
L	linear dimension
L_s	length scale factor
l	linear reference dimension of the path of a snow particle
m	mass of particle
$P(,)$	probability of (,)
R	radius of tube
Re	Reynolds number
Re_d	Reynolds number based on particle diameter
rms	root-mean-square
r	radius of particle
S	defined by eq 17
S_a	cross-sectional area of particle
t	time
U_s	velocity scale factor
\bar{u}	mean velocity of flow through tube
v	velocity and velocity components of particles used in "Particle-field interaction"

LIST OF SYMBOLS (Cont'd.)

V	velocity of air or fluid in general
V_f	particle fall velocity
V_{ft}	particle free-fall velocity
V_m	wind-tunnel air velocity
V_p	particle velocity
V_r	relative velocity of particle to wind
V_t	threshold velocity
V_*	friction velocity
V_{*t}	threshold friction velocity
V_∞	free-stream velocity
x	horizontal coordinate oriented downwind
x_0	horizontal coordinate of a fixed point in space
$\dot{x}(0)$	initial x-component of particle velocity
y	vertical coordinate oriented upward
y_0	vertical coordinate of a fixed point in space
$\dot{y}(0)$	initial y-component of particle velocity
y^*	top of the boundary layer
α	angle defined in Figure 6
β	angle between drag force and horizontal (Fig. 1a)
β_s	scattering angle; initial angle of particle velocity relative to the horizontal (Fig. 6)
γ	transverse angular range of approaching particle
λ	coefficient of resistance
μ	viscosity
ν	kinematic viscosity
ρ	fluid or air density
ρ_p	particle mass density
Σ	particle-diameter scale factor
σ	particle diameter
τ_0	fluid shear stress at the surface
ψ	angle of approach particle to surface
$()_h$	horizontal component
$()_i$	end values in trajectory
$()_m$	model variables
$()_n$	normal component
$()_0$	initial values in trajectory

LIST OF SYMBOLS (Cont'd.)

$()_t$	tangential component
$()_v$	vertical component
$()_{1,2,\dots}$	particle identification index
$()_\infty$	free-stream quantity
$()_{00}$	most probable values
$(\dot{})$	differentiated with respect to time
$(\ddot{})$	twice differentiated with respect to time
$()'$	quantity after collision

SCALE MODEL STUDIES ON SNOW DRIFTING

by

Gordon H. Strom, George R. Kelly,
Edwin L. Keitz and Robert F. Weiss

INTRODUCTION

One of the more troublesome features of arctic life has been the serious handicap imposed on all forms of activity by blowing and drifting snow. Over the years man has developed techniques to gain partial control of this phenomenon. Such devices as snow fences probably were evolved from observation of the effect of such natural windbreaks as hedgerows on snow drifting and owe their design more to local availability of materials than to aerodynamical or meteorological considerations. The snow fences used in various countries differ considerably in form. It is difficult to account for the particular configuration which is in local use except that it is traditional and low in cost.

One of the reasons for the absence of more conscious design in the development of snowdrift control methods has been the necessity and difficulty of field testing any newly conceived model over a period of years in order to observe its performance over a full range of meteorological conditions. However, a few decades ago, the idea of using a wind tunnel to test such designs, with consequent savings in time and cost, occurred to people in several snow countries. E. A. Finney (1940) in Michigan performed a variety of wind tunnel experiments using balsa sawdust and mica flakes to represent snow. From these he drew a number of interesting conclusions about the sizes of turbulent regions in relation to the obstacles which produced them. The results of his studies have been found very useful by people working on highway design and maintenance.

In Scandinavian countries also there was interest in wind-tunnel experimentation on blowing snow. C. Nokkentved (1938) performed similar experiments and obtained results which were in general accord with Finney's findings. Becker (1944) conducted a few tests in Germany, but later despaired of obtaining entirely satisfactory results from such investigations in view of the seemingly insurmountable problems of

- (a) simulating the snow adequately, and
- (b) satisfying the scaling criteria accurately.

S. Hallberg and others (1943) of the State Road Institute of Sweden investigated the eddies around snow fences, using full-scale fences in the out-of-doors with silk streamers to define the flow patterns.

These investigations proved to be quite useful in establishing certain gross concepts of snow blowing and drifting behavior, but all of them suffered from the difficulties noted by Becker. In general, the materials used to simulate snow were chosen arbitrarily, based upon such secondary considerations as cost, availability, or superficial likeness to actual snow. Although the necessity for scaling the structures represented was recognized, little was done to insure that the particles of blowing snow were scaled in proportion. Consequently, the end result was a little like examining the behavior of flying baseballs as a basis for drawing conclusions on the behavior of blowing snow.

Dr. R. W. Gerdel (1960) of U. S. Army Snow, Ice and Permafrost Research Establishment, * pointed out that it is essential to scale the dimensions and physical properties of the material simulating snow in wind tunnel investigations in order to gain true similitude to the behavior of the snow.

The present project resulted from this suggestion and had as its goal the investigation of the micro-meteorological factors which control the drifting of snow, with the special objective of determining a material which can be used in the wind tunnel to represent the behavior of snow accurately.

* Redesignated U. S. Army Cold Regions Research and Engineering Laboratory,
1 February 1961.

THEORETICAL ANALYSIS OF SALTATION PHENOMENA IN SNOW DRIFTING

The details of snowdrifting phenomena are so complex that it is difficult to obtain an understanding of the fundamental mechanism involved by either theoretical or experimental methods. A combination of the theoretical and experimental approaches is likely to yield more progress than either one alone. The following section presents a theoretical analysis of an important phase of snow drifting and adds to the understanding of the fundamental mechanism.

Pioneering work in drifting problems has been carried out by Bagnold (1941), who provides basic descriptions of the various significant phenomena. The transport of small particles over a surface has been shown to consist of suspension, saltation, and surface "creep" of the material involved. In the application of drifting problems to snow, particle-surface interactions are of primary interest. The larger part of particle transport over a surface has been shown to be due to saltation, or bouncing of particles from point to point in the general direction of the free stream. Hence, it is logical to first consider the saltation process and attempt to obtain reasonable results for a specific physical model. Such results should include a predicted "wave length" of drifting and vertical particle distribution in the saltation layer.

The analysis consists of three fundamental subjects: (1) analysis of the movement of a particle through the air, between interactions with the surface, (2) description of a particle field on the surface, and interaction of an airborne particle with the field; and (3) a correlation between these phenomena that will provide a steady-state solution to the particle distribution.

Development of theoryAssumptions.

1. Particles are elastic, spherical, equally sized, and much smaller than the boundary layer thickness.
2. Field consists of a special closely packed geometrical arrangement of particles, free to move in the plane of the field only.
3. Phenomena are investigated at points sufficiently far downstream to allow a large number of particles to reach "equilibrium" with the field.
4. Only primary interactions are considered, secondary "ejections" being shown to comprise a small fraction of the total saltation.
5. Rolling particles, randomly located, initiate saltation at all points on the field.
6. In-air collisions of particles, boundary layer turbulence, and crosswind are neglected.

Trajectory analysis. Figure 1 shows the relationship between velocities and forces on a particle at any time during its trajectory and Figure 2 shows the simplified boundary layer employed to facilitate solution of equations of motion. V is a linear function of y within the boundary layer depth y^* . The assumption is valid if the particle does not pass above y^* , and is generally indicative of a laminar sublayer to the turbulent atmospheric boundary layer.

The following two equations are formed by setting the sums of forces equal to particle mass times its accelerations in the x and y directions. y is taken vertically upward. D_g is the aerodynamic drag force which acts in the direction opposite to relative velocity \bar{V}_p of the particle and surrounding air. mg is particle weight.

$$D_g \sin \beta - mg = m\ddot{y} \quad (1)$$

$$D_g \cos \beta = m\ddot{x}. \quad (2)$$

The velocities are related to the angle β by the following equation where \dot{y} is the vertical component of particle velocity:

$$\sin \beta = -\dot{y}/V_r.$$

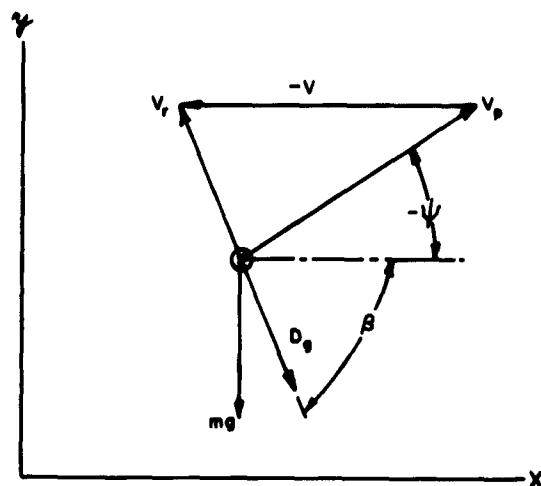


Figure 1. Forces and velocities of a particle.

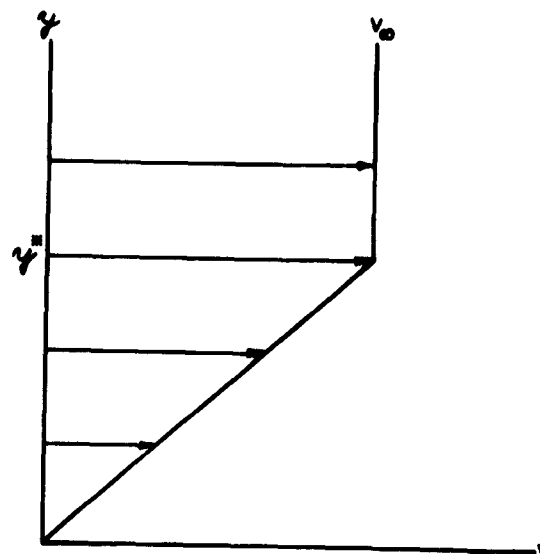


Figure 2. Linear velocity profile assumed for boundary layer.

At the low Reynolds numbers encountered in these particle motions, the drag force is approximately proportional to relative velocity as follows:

$$D_g = k_0 V_r. \quad (3)$$

The left side of eq 1 becomes

$$D_g \sin \beta = -k_0 V_r \dot{y} / V_r = -k_0 \dot{y}$$

and eq 1 becomes

$$\ddot{y} + (k_0/m)\dot{y} + g = 0. \quad (4)$$

In eq 4, taking the Laplace transform of both sides,

$$s^2 f(s) - \dot{y}(0) + \frac{k_0}{m} s f(s) + \frac{g}{s} = 0$$

which is simplified to:

$$f(s) = -\frac{mg}{k_0} \left\{ \frac{1 + \left(\frac{-\dot{y}(0)}{g} \right) s}{s^2 \left(1 + \frac{m}{k_0} s \right)} \right\}$$

taking the inverse transform:

$$f(t) = y = \frac{mg}{k_0} \left\{ \left[\frac{\dot{y}(0)}{g} + \frac{m}{k_0} \right] \left[1 - e^{-(k_0/m)t} \right] - t \right\}. \quad (5)$$

Equation 2 is now written

$$k_0 V_r \cos \beta = m \dot{x}$$

where

$$\cos \beta = \frac{V - \dot{x}}{V_r};$$

therefore,

$$\frac{k_0 V_r}{V_r} [V - \dot{x}] = m \dot{x}$$

or

$$\dot{x} + (k_0/m)\dot{x} = (k_0/m)f_1(t) \quad (6)$$

since V can now be expressed as $f_1(t)$.

In operator form, eq 6 becomes:

$$[D^2 + (k_0/m)D]x = (k_0/m)f_1(t)$$

or

$$D[D + (k_0/m)]x = (k_0/m)f_1(t).$$

$$\text{Letting } [D + (k_0/m)]x \equiv H; \quad DH = (k_0/m)f_1(t).$$

Substituting

$$k_1 y = V(y) = f_1(t),$$

$$DH = k_1 \left[\dot{y}(0) + mg/k_0 \right] \left[1 - e^{-(k_0/m)t} \right] - gk_1 t \quad (7)$$

which, when integrated, yields

$$H = k_1 \left[\dot{y}(0) + mg/k_0 \right] \int \left[1 - e^{-(k_0/m)t} \right] dt - gk_1 \int t dt$$

and

$$(D + k_0/m)x = k_1 \left[\dot{y}(0) + mg/k_0 \right] \left[t - (m/k_0)e^{-(k_0/m)t} \right] - gk_1 t^2/2 + C_1.$$

This is a linear equation, having the solution:

$$x = e^{-(k_0/m)t} \int e^{(k_0/m)t} \left\{ k_1 \left[\dot{y}(0) + mg/k_0 \right] \left[t + (m/k_0)e^{-(k_0/m)t} \right] + C_1 - k_1 g t^2/2 \right\} dt + C_2 e^{-(k_0/m)t}. \quad (8a)$$

Integrating eq 8a by parts gives:

$$x = k_1 A \left[\frac{t}{B} (e^{-Bt} + 1) - \frac{1}{B^2} \right] - \frac{k_1 g}{2} \left[\frac{2}{B^3} + \frac{t^2}{B} - \frac{2t}{B^2} \right] + C_2 e^{-Bt} + \frac{C_1}{B} \quad (8b)$$

where $B = k_0/m$ and $A \equiv \left[\dot{y}(0) + \frac{g}{B} \right]$.

From the boundary conditions

$x = 0, \dot{x} = \dot{x}(0)$ at $t = 0$; we get, finally:

$$x = k_1 A \left[\frac{t}{B} (e^{-Bt} + 1) - \frac{1}{B^2} \right] - \frac{k_1 g}{2} \left[+ \frac{2}{B^3} + \frac{t^2}{B} - \frac{2t}{B^2} \right] + \left[\frac{k_1 g}{B^3} + \frac{2k_1 A}{B^2} - \frac{\dot{x}(0)}{B} \right] e^{-Bt} + \left[\frac{\dot{x}(0)}{B} - \frac{k_1 A}{B^2} \right] \quad (9)$$

which, when combined with eq 5, gives a parametric description of the position of a particle.

$$\text{Let } C = \frac{k_1 g}{B^3} + \frac{2k_1 A}{B^2} - \frac{\dot{x}(0)}{B}$$

and form the derivatives of y and x with t as follows

$$\frac{dx}{dt} = \frac{k_1 A}{B} \left[e^{-Bt} (1 - Bt) + 1 \right] - \frac{k_1 g}{B} \left[t - \frac{1}{B} \right] - BC e^{-Bt}$$

$$\frac{dy}{dt} = A e^{-Bt} - \frac{g}{B}$$

and the angle of inclination of the particle velocity, ψ , is given by:

$$\tan \psi = \frac{dy}{dx} = \frac{dy/dt}{dx/dt} = \frac{A e^{-Bt} - g/B}{\frac{k_1 A}{B} \left[e^{-Bt} (1 - Bt) + 1 \right] - \frac{k_1 g}{B} \left[t - \frac{1}{B} \right] - BC e^{-Bt}} \quad (10)$$

This quantity will be useful in the following interaction analysis.

Particle - field interaction. The most important assumption here concerns the "model" snowfield to be used. For simplicity of analysis (with good approximation to the physical situation), a "closely packed" field is assumed (Fig. 3). Such a field seems quite arbitrarily oriented as far as an approaching particle is concerned, and it is also reasonable to assume that field particles, though close to each other, do not touch in general. The field particles are then free to move in the plane of the surface, but are assumed to meet infinite resistance normal to the surface. Furthermore, an approaching particle has two important restrictions on its interaction with the field:

a. The maximum angle of approach off a stationary particle's centerline (in transverse plane) is limited to 30° (Fig. 4). Particles approaching as far off center as shown in the figure will be only slightly deflected, because the large transverse deflection angle is opposed by a small transverse velocity (compared to longitudinal velocity). Thus, an essentially two-dimensional interaction may be assumed: i. e., spheres impacting on cylinders placed normal to the free stream.

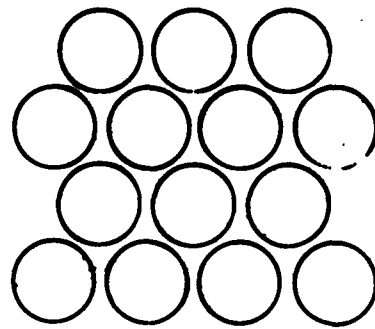
b. The minimum distance between centers of approaching and stationary particles is a function of the angle of approach (Fig. 5). This may be expressed as,

$$\sin \psi = \frac{n}{\sigma} \text{ and } b_{\min} = \sigma - n = \sigma - \sigma \sin \psi \quad (11)$$

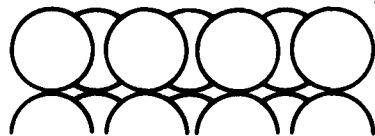
$$b_{\min} = \sigma (1 - \sin \psi)$$

a relationship to be used in actual calculation.

Finally, it should be pointed out that a typical occurrence in saltation is the ejection of new particles from the surface. This is indeed possible in the model field set up, as a struck particle is free to move until striking an adjacent particle, whereupon it will rebound into the airstream. Many more particles will, in turn, be struck, but the



TOP VIEW



FRONT VIEW

(LOOKING DOWNSTREAM)

Figure 3. Assumed form of particle field at surface.

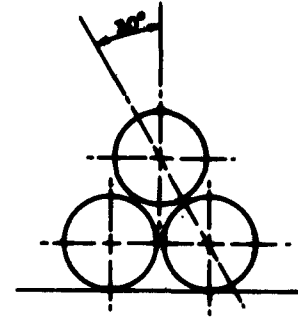


Figure 4. Maximum transverse angle of approach is shown to be 30°. (Front view looking downstream.)

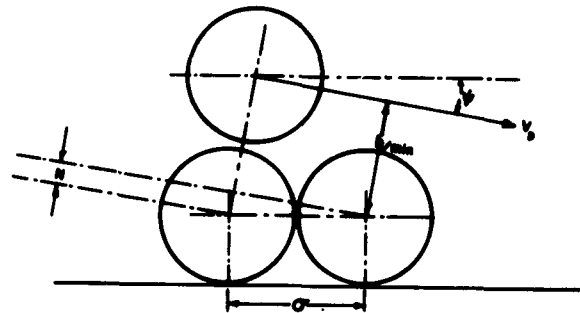


Figure 5. Interaction limitations.

loss of energy in an interaction is so great that even the secondary interaction results in very small ejection velocities. In the analysis to follow, only primary interactions are considered, but these procedures could be extended to include secondary effects.

In the following analysis, equations are developed which relate the velocities and path angles of a particle before and after impact for one degree of freedom. The imperfectly elastic properties are expressed in terms of the coefficient of restitution. The designations of velocities before and after impact are shown in Figure 6.

Since the total momentum of the approaching particle's normal velocity component may be divided into horizontal and vertical components, we may say that the change in momentum of the impacting particle equals the sum of the changes of its components. In this analysis, we of course assume a smooth surface and smooth particle. Hence, v_{1t} is preserved and equals v'_{1t} . The vector diagrams before and after interaction are shown in Figure 6 where primes denote post-collision quantities, and β_s is scattering angle.

The velocities before and after collision are related to the coefficient of restitution e , which is defined by:

$$e = \frac{v'_a - v'_b}{v_b - v_a} \quad (12)$$

The respective particles are indicated by the subscripts a and b .

When applied to the horizontal components, the following is the result:



AFTER

$$v'_{1nh} = \frac{v_{1nh}}{1 + \left(\frac{1+e}{1-e} \right)}.$$

(13)

In the vertical direction, \underline{m}_2 is assumed infinite because of the resistance to motion normal to the surface, so that $v_2 = v_2' = 0$ and

$$e = v_1' / (-v_1)$$

or

$$\mathbf{v}_1' = -e\mathbf{v}_1.$$

When applied to the vertical component, $(v'_2 - v'_0)$ and $(v_0 - v_2)$ are the separating and closing velocities, respectively, of the two particles. Since there is no resistance to particle "2" movement at impact, the conservation of momentum gives in general form

$$v_1 + v_2 = v'_1 + v'_2 = v_1;$$

$v_2 = 0$ since particle "2" is initially at rest. The coefficient of restitution gives

$$e = \frac{v'_1 - v'_2}{-v_1}.$$

Solving for velocity v'_1 in terms v_1 gives:

$$v'_1 = \frac{v_1}{1 + \frac{1+e}{1-e}}$$

$$v'_{1nv} = -ev_{1nv}. \quad (14)$$

From Figure 6, we may write:

$$\tan \beta_s = \frac{v'_{1nv} + v'_{1t} \sin \left[\frac{\pi}{2} - (\alpha + \psi) \right]}{v'_{1t} \cos \left[\frac{\pi}{2} - (\alpha + \psi) \right] + v'_{1nh}} \quad (15)$$

where $\alpha = \sin^{-1} \frac{b}{\sigma}$, as seen in the figure,

$$\text{and, of course, } \sin \left[\frac{\pi}{2} - (\alpha + \psi) \right] = \cos (\alpha + \psi)$$

$$\cos \left[\frac{\pi}{2} - (\alpha + \psi) \right] = \sin (\alpha + \psi).$$

$$\text{Now, since } v_{1nv} = v_1 \cos \alpha \sin (\alpha + \psi) \quad (16)$$

$$v_{1nh} = v_1 \cos \alpha \cos (\alpha + \psi)$$

$$\text{and } v_{1t} = v_1 \sin \alpha$$

$$\text{and defining } S = 1 + \frac{1+e}{1-e},$$

we obtain

$$\tan \beta_s = - \left[\frac{eS \tan (\alpha + \psi) + S \tan \alpha}{S \tan \alpha \tan (\alpha + \psi) + 1} \right]. \quad (17)$$

Particle distribution. With a uniform density of I_0 particles/sec-unit area impacting on a field particle, the total number/sec passing through an annular ring at a distance b (see Fig. 7), db wide is dN ; and,

$$dN = I_0 \gamma b db$$

$$\text{where } \gamma = \text{angular range about center.} \quad (18)$$

Since particles impacting at a distance b rebound at the angle β_s , dN is the number of particles/sec rebounding at angles between β_s and $\beta_s + d\beta_s$. We must now compute b , or α , and db in terms of β_s and the other relevant parameters.

Differentiating both sides of eq 17 with respect to α , and noting that $d(\alpha + \psi) = d\alpha$, we get

$$db = \frac{\sqrt{\sigma^2 - b^2} \sec^2 \beta_s d\beta_s [S \tan \alpha \tan(\alpha + \psi) - 1]}{S \left\{ \sec^2(\alpha + \psi) [e + S \tan^2 \alpha] + \sec^2 \alpha [1 + eS \tan^2(\alpha + \psi)] \right\}} \quad (19)$$

Using $\tan(\alpha + \psi) = \frac{\tan \alpha + \tan \psi}{1 - \tan \alpha \tan \psi}$, we may rewrite eq 17 as:

$$\tan^2 \alpha [S \tan \beta_s - S \tan \psi] + \tan \alpha [(S-1) \tan \psi \tan \beta_s + S(e+1)] + [\tan \beta_s + eS \tan \psi] = 0 \quad (20)$$

a quadratic in $\tan \alpha$, which may be solved to give the required relationship for $b = b(\beta_s, \text{etc.})$, i. e.,

$$\tan \alpha = \frac{-B \pm \sqrt{B^2 - 4AC}}{2A} \quad \text{and} \quad \tan \alpha = \frac{b}{\sqrt{\sigma^2 - b^2}}.$$

We may now express the number of particles rebounding per sec per unit angle β_s as

$\frac{dN}{d\beta_s} = K_2 F(\beta_s, \psi, e, \sigma)$ and call this quantity the probability that a particle will rebound at an angle β_s , having approached the field at angle ψ . Incorporating K_2 , a constant, into this probability (since I_0 is unknown anyway), we have obtained

$$P(\beta_s, \psi) = f(\beta_s, \psi, e, \sigma). \quad (21)$$

For purposes of comparing this probability function with those for the well known cases of infinite restraint and zero restraint (in all directions), we let $\psi = 0$ and $e = 1$. The results are shown in Figure 8.

Having obtained the trajectory and surface interaction relationships, we attempt to correlate this information to obtain the fundamental unknown in the problem, $P(\beta_{s_0}, v_0')$, the probability that a particle will leave the surface at an angle β_{s_0} and velocity v_0' . The particle distribution above the surface may then be calculated and the "wave length" of the saltation phenomenon estimated.

Correlation. The following notation will be used:

- β_{s_0}, v_0' are angle and velocity at beginning of a trajectory (initial values)
- ψ, v_1 are angle and velocity at end of trajectory
- β_{s_1}, v_1' are angle and velocity after interaction, hence are initial values of next trajectory.

The main assumption employed here is as follows: If there is any set of probabilities $P(\beta_{s_0}, v_0')$ that exist at various values of x , and are invariant in time, because of a boundary condition at x_0 , we see that the same set exists at point $x + \Delta x$ because of the same boundary conditions at $x_0 + \Delta x$. The boundary conditions are, in fact, duplicated at $x_0 + \Delta x$ (for all values of Δx) in a field of randomly originating rolling particles. Hence, all possible member of the P -set are superimposed at all x 's sufficiently far downstream, and we can assume the sum of these to equal the $P(\beta_{s_0}, v_0')$, that is invariant with respect to both time and x . This argument reduces to the assumption that

$$P(\beta_{s_1}, v_1') = P(\beta_{s_0}, v_0') = P(\beta_s, v'). \quad (22)$$

We now look at a set of trajectories terminating at a fixed point x , each trajectory being determined uniquely by specifying ψ and v_1 . We then assume the existence of a $P(\psi, v_1)$, the probability that a particle will terminate its trajectory at angle ψ and velocity v_1 . Then, since v_1 is related to v_1' and β_{s_1} , there is a determinable number of particles/sec terminating at ψ and a v_1 such that the percentage rebounding at β_{s_1} will have velocity v_1' . The percentage rebounding at β_s , is, of course, $P(\beta_{s_1}, \psi)$, as already obtained. If we

sum over-all values of ψ , we obtain the total number/sec rebounding at β_{s1} and v_1' , or $P(\beta_{s1}, v_1')$. Finally, we note that the number of particles at ψ and v_1 equals the number having left the surface at values of β_{s0} and v_0' , determined by relationships derived in Figure 6. Thus,

$$P(\beta_{s1}, v_1') = \int_{\psi_{\min}}^{\psi_{\max}} P(\beta_{s0}, v_0') P(\beta_{s1}, \psi) d\psi \quad (23)$$

where β_{s0} and v_0' are functions of ψ , β_{s1} and v_1' .

The required relationship between v_1 and v_1' , mentioned above, is now derived.

From Figure 8 we see that:

$$(v_1')^2 = [v_{1nv}' + v_{1t}' \cos(\alpha + \psi)]^2 + [v_{1t}' \sin(\alpha + \psi) + v_{1nh}']^2$$

and, with substitutions as before,

$$v_1' = E \frac{1}{2} v_1 \quad (24a)$$

$$\text{where } E = [e \cos \alpha \sin(\alpha + \psi) + \sin \alpha \cos(\alpha + \psi)]^2 + [\sin \alpha \sin(\alpha + \psi) + \frac{1}{5} \cos \alpha \cos(\alpha + \psi)]^2. \quad (24b)$$

Finally, since $v_{1y} = v_1 \sin \psi$,

$$v_1 = \frac{[v_0' \sin \beta_{s0} + \frac{g}{B}] e^{-B t_0} - \frac{g}{B}}{\sin \psi} \quad (25)$$

where t_0 is the terminal time.

Program for numerical solution. The program that must be followed for numerical solution of the problem is now outlined:

- (1) β_{s1} and v_1' are chosen arbitrarily.
- (2) α is determined from eq 20 for various ψ 's.
- (3) E and v_1 are calculated from eq 24a and 24b for various ψ 's.
- (4) $y(0)$ is calculated from eq 25 for various ψ 's.
- (5) $x(0)$ is calculated from eq 10 for various ψ 's.
- (6) then β_{s0} , v_0' are easily calculated for various ψ 's.
- (7) $P(\beta_{s1}, \psi)$ is determined from eq 21 for various ψ 's.
- (8) $P(\beta_{s0}, v_0')$ is assumed to be of the simple gaussian-type form:

$$P(\beta_{s0}, v_0') = (\beta_{s0}, v_0')^2 e^{-\left[\frac{\beta_{s0}}{C_3} + \frac{v_0'}{C_4}\right]} \quad (26a)$$

where C_3 and C_4 are constants to be determined, equal to the one-half the most probable angle β_{s00} and one-half the most probable velocity v_{00}' , respectively; i. e.,

$$\text{when } \frac{\partial P}{\partial \beta_{s0}} = 0, \frac{\partial P}{\partial v_0'} = 0, \beta_{s0} = 2C_3 = \beta_{s00} \quad (26b)$$

$$v_0' = 2C_4 = v_{00}'.$$

Assuming C_3 and C_4 , $P(\beta_{s0}, v_0')$ is calculated.

- (9) The product $P(\beta_{s0}, v_0') P(\beta_{s1}, \psi)$ is then integrated over ψ using Simpson's rule; i. e.,

$$P(\beta_{s_1}, v_1') = \frac{\psi_n - \psi_0}{3n} [\psi_0 + 4(\psi_1 + \psi_3 + \dots) + 2(\psi_2 + \psi_4 + \dots) + \psi_n]. \quad (27)$$

(10) $P(\beta_{s_1}, v_1')$ is calculated independently from eq 26a and the result compared to eq 27.

(11) Adjustment of C_3 and C_4 is made until the values obtained in eq 9 and 10 are equal. Since each constant can be independently adjusted until this requirement is met, it is necessary to plot C_3 vs C_4 for two distinctly different sets of β_{s_1} and v_1' values. The intersection of these two curves is assumed, without proof of uniqueness, to be the solution, i. e., $\beta_{s_{00}}$ and $v_{0'0}$.

(12) Since we are dealing with saltation only, and assuming this phenomenon to be most responsible for small-scale "drifting" (no large surface obstructions), it seems reasonable to assume that any event occurring on the field will be duplicated a distance downstream corresponding to the "most probable" trajectory. This trajectory is determined by $\beta_{s_{00}}$ and $v_{0'0}$, and its "range" may be interpreted as the propagation wave length. It is calculated with eq 9.

(13) The vertical particle distribution in the saltation layer may now be obtained:

a) y_0 , the height above the surface is chosen, as are several evenly spaced distances, Δx_0 , upstream of the location in question.

b) For various t_0 's (corresponding to the position of a particle at y_0 , Δx_0) $\dot{y}(0)$ and $\dot{k}(0)$ are calculated from eq 5 and 9, respectively; $-y_0$ and x_0 are fixed here.

c) Having β_{s_0} and v_0' for various t_0 's, we plot β_{s_0} vs v_0' , and repeat this procedure for other Δx_0 values.

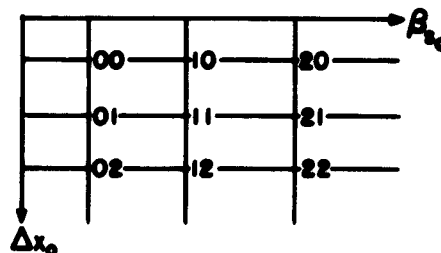
d) Now, for each Δx_0 , we may calculate $P(\beta_{s_0}, v_0')$ as a function of β_{s_0} , and we essentially have $P(\beta_{s_0}, \Delta x_0)$, describing the number of particles emitted at Δx_0 such that they must all pass through the point y_0 above the surface. Integration over Δx_0 gives the total number of particles passing through y_0 , x_0 ; i. e.,

$$N_{x_0, y_0} = \int_0^{x_0} \max \int_0^{\frac{\pi}{2}} P(\beta_{s_0}, \Delta x_0) d\beta_{s_0} d(\Delta x_0) \quad (28)$$

which may be evaluated by Simpson's rule for two independent variables. For nine known values this becomes:

$$N_{x_0, y_0} = \frac{h^2}{9} \{ 16P_{11} + 4[P_{10} + P_{01} + P_{12} + P_{21}] + P_{00} + P_{02} + P_{22} + P_{20} \} \quad (29)$$

h refers to interval subdivision size (since units are different for β_{s_0} and Δx_0 , $h \equiv 1$ is acceptable for purposes of comparison at different y_0 's), and P_{ij} indicates values of $P(\beta_{s_0}, \Delta x_0)$ at the station ij as shown below:



e) N_{x_0}, y_0 is calculated for several y_0 's and the relative magnitude of these values may be taken as the particle distribution at an arbitrary point far downstream.

Several details should also be included in the program just outlined:

- a) In the quadratic expression defining α , only one solution, the negative angle, is physically possible (because of the presence of a surface).
- b) Limits are imposed on ψ by both the maximum attainable vertical (terminal) velocity and the interference of surrounding field particles (see eq 11), remembering that β_{s1} depends on b , and b_{\min} is a function of ψ .
- c) Because of the existence of a terminal velocity (and secondarily because of inelastic impacts), there is a maximum height to the saltation layer and a maximum velocity attainable by any particle. This maximum velocity could be calculated, but in this study, for purposes of comparison, it is assumed at all times to be equal to the vector sum of the free stream and terminal velocities.
- d) From the vector diagram $\beta_{su} \leq 90^\circ$; it cannot be "specified" larger.

Numerical example

As yet an undecided question is the possibility of writing drag as $k_0 V_r$. Since the particle is not at rest in any part of the trajectory analysis, we may consider the Reynolds no. range from 10^{-1} to 10^{+2} , in which values of C_D , the drag coefficient, are obtained from Hoerner (1958) (C_D for the sphere). And, assuming $C_D = 100/Re_d$, we obtain a reasonable approximation to the experimental variation. Then,

$$k_0 = \frac{1}{2} \rho C_D S_a V_r = \frac{1}{2} \rho S_a \left(\frac{100 \mu}{\rho \sigma V_r} \right) V_r = \frac{50 \pi}{4} \mu \sigma.$$

For purposes of future experimental verification, the following set of physical data was assumed:

1. particle density = 100 lb/ft³ (commercial glass spheres)
2. particle coefficient of restitution = 0.94
3. particle diameter = 0.2 mm.
4. boundary layer: linear variation to 15 ft/sec in 6 in.; i. e., $k_0 = 30$ (standard atmosphere assumed).

A trajectory was traced out (Fig. 9) using possible values for β_{s0} and v'_{00} . This path appears quite reasonable when compared to photographs obtained by Bagnold (1941) for sand.

The analysis outlined above (p. 2-5) gave the following results:

- a) $\beta_{s00} = 5^\circ$, $v'_{00} = 8.6$ ft/sec; $P(\beta_{s0}, v'_0)$ given in Figure 10.
- b) The "ripple wave length" was then calculated to be 1.6 in.
- c) The particle number density, calculated at four points, is represented in Figure 11 as a vertical distribution with arbitrary reference value.

These results are also quite reasonable when compared with tests using borax of nearly 0.2 mm average diameter and similar density. The major objection to such a comparison is the lack of sphericity in these particles. However, it is possible to assume an equivalent statistical diameter for rotating prismatic shapes (during trajectory) equal to

$\frac{\sigma_{\max}}{2}$, an rms value. This question must be investigated further, and more conclusive results will be obtained from the proposed tests with glass spheres.

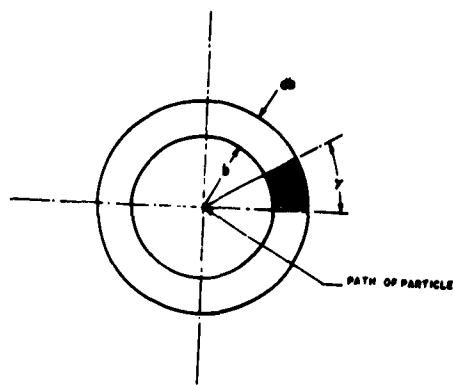


Figure 7. Definition of area for particle impact used in eq 18. View taken in direction of particle path.

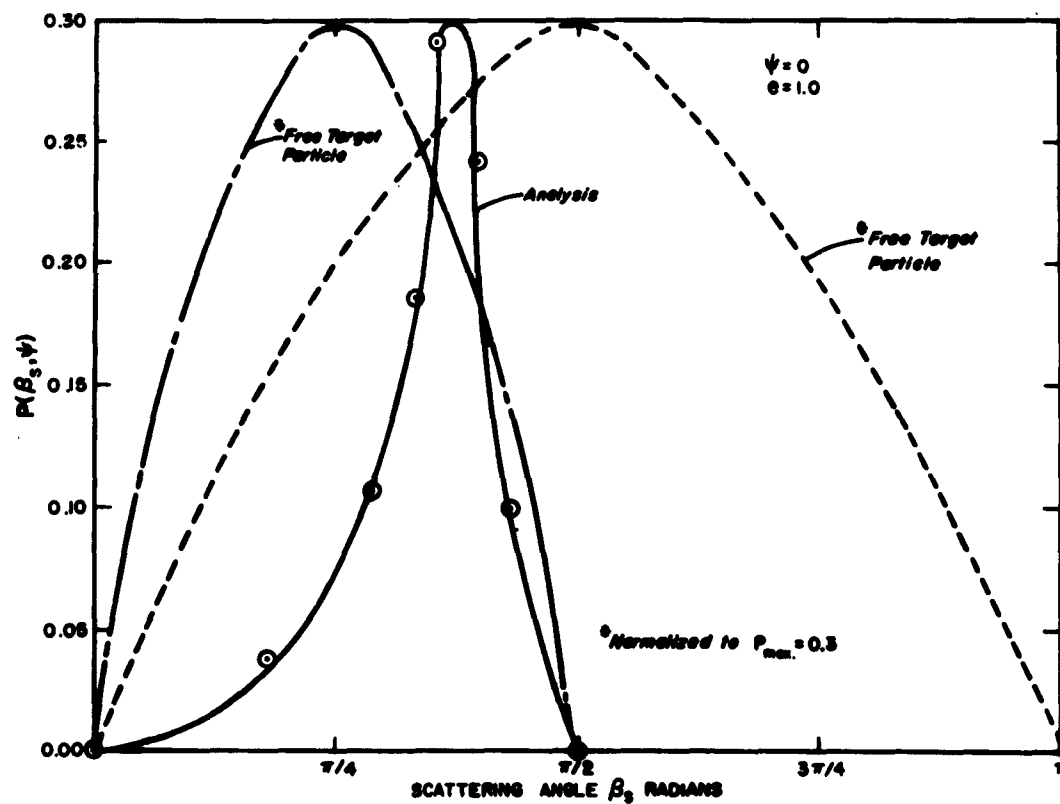


Figure 8. Probability of scattering angle β_s .

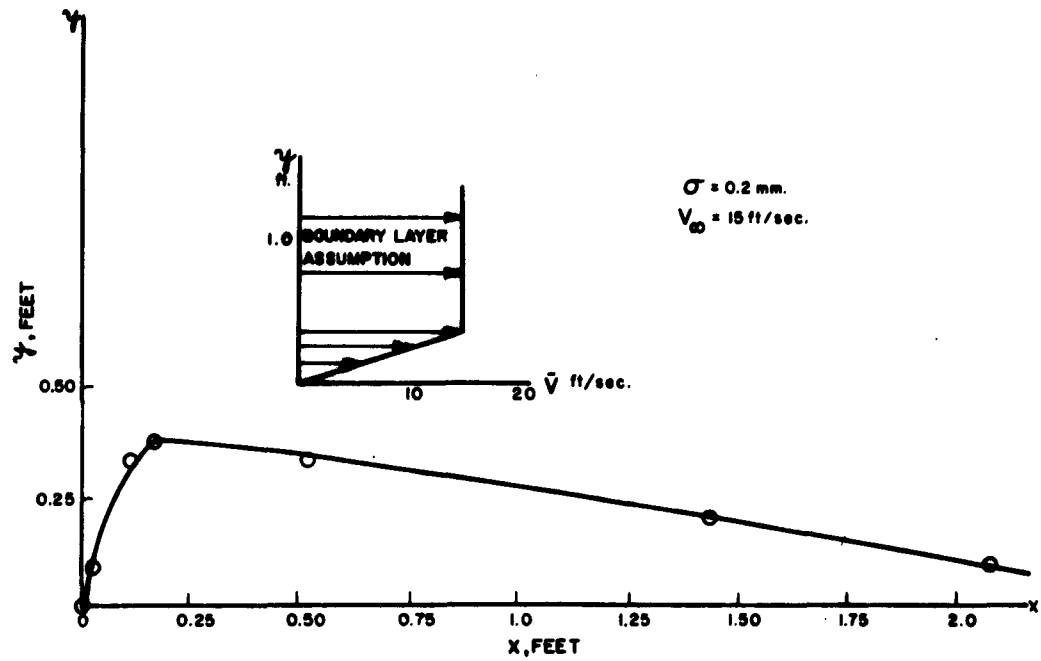


Figure 9. Typical trajectory for glass sphere.

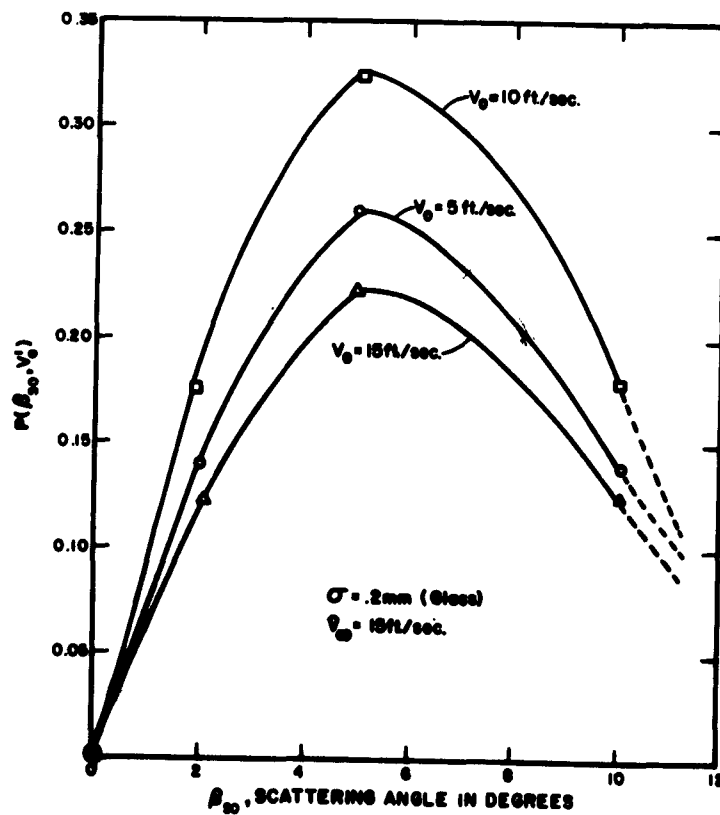


Figure 10. Probability of initial angle and velocity.

A numerical example such as this serves to indicate the plausibility of the analysis as carried out thus far, and also points up the desirability of either simplifying the equations or programming them for automatic computation.

Summary of analysis of saltation phenomenon

a) While certain physical and mathematical assumptions are still open to question, the quantitative analysis of the saltation layer is both feasible and physically meaningful.

b) The analysis should be extended, approximately, to particles with non-spherical shape and variations in diameter.

c) The variation of all results with changes in boundary layer and field arrangement assumptions should also be investigated.

d) The effects of obstructions must be considered together with those of wavy surfaces in an effort to determine the stable profile shape of a snow surface. Many interesting confirmatory experiments are possible in this phase of the study.

e) Results of this and subsequent analyses should ultimately be applied to the detailed formulation of modeling criteria. Thus, for example, if it is particle distribution and wave configuration that must be duplicated in scale model experiments, it would be possible to determine the required scale factors to achieve this. Scale experiments then would afford the best means of time studies of large-scale drifting and accumulation.

DEVELOPMENT OF SCALE FACTORS

Scale factors based on dimensional analysis

The complex nature of snow-drifting phenomena makes the determination of modeling criteria especially difficult. Conflicting requirements are encountered and it must be decided which may be neglected without serious loss of accuracy. Those criteria which appear most important at this time are presented in the following section. Further experience with snow-drift modeling will undoubtedly lead to improvements in modeling criteria.

Scale factors for establishing modeling criteria will be developed by two methods. Dimensional analysis will be the primary basis for the first method, while the equations of motion of a particle will be used in the second. The latter covers part of the scale factors developed by the first method.

The development of the scale factors will be carried out in steps based on various phases of snow-drifting phenomena. Most of the scale factors will be developed by dimensional analysis but some will be based on characteristics of the physical phenomena involved.

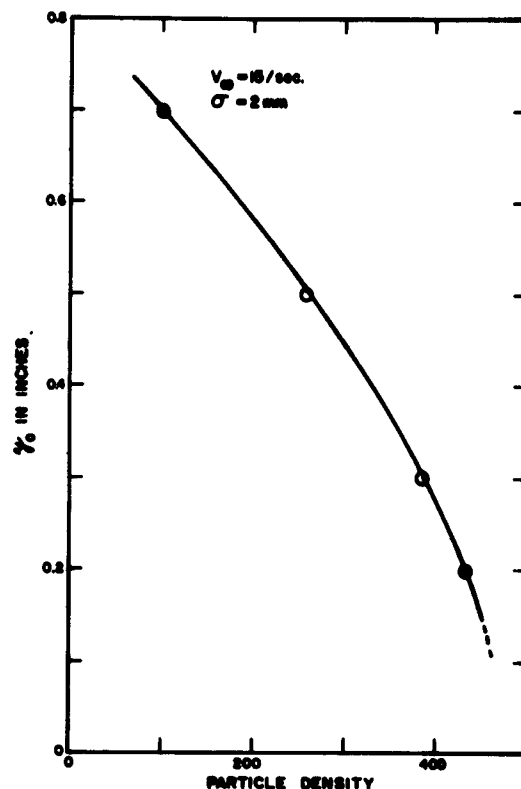


Figure 11. Particle distribution.

At this stage of development, it appears advisable to concentrate on modeling of geometric properties. It is certainly necessary to preserve geometric configuration of snow drifts and for many applications this may be the most important characteristic. Modeling of other properties such as mass transport and density of snow in suspension may be achieved automatically if geometric similarity of detailed characteristics of the phenomena are preserved, particularly the paths or trajectories of individual particles. Similarity of paths will be the basis for the following analysis. It is obvious that similarity of paths will have little significance unless there is also geometric similarity of the rigid boundaries such as buildings, snow fences, roadways, etc. It will be assumed that such similarity exists, although it could be included in the analysis.

Snow drifting is known to occur in three phases: namely, suspension, saltation, and creep. The scale factors which are significant to the suspension phase will be considered first. A snow particle will be treated as being in a path or trajectory influenced only by fluid and gravitational forces. The following nine variables are considered as significant:

- L = linear reference dimension of rigid boundary objects
such as buildings and snow fences
- l = linear reference dimension of the paths of a snow particle
- σ = diameter of snow particle
- m = mass of snow particle
- V_p = velocity of snow particle
- V = ambient air velocity at the particle
- ρ = air density
- μ = coefficient of viscosity for air
- g = acceleration due to gravity.

The following equation is formed by employing the six dimensionless products which may be developed by dimensional analysis from the above variables.

$$\frac{l}{L} = f\left(\frac{\sigma}{L}, \frac{V_p^2}{g\sigma}, \frac{m}{\rho\sigma^3}, \frac{V_p}{V}, \frac{V_p\rho\sigma}{\mu}\right) \quad (30)$$

l/L may be interpreted as a measure of geometric similarity of particle path to rigid boundaries as well as the ratio of their linear dimensions. On the basis of the above equation, similarity of snow particle paths is preserved if each of the five dimensionless products on the right side of the equation are maintained at the same value in the model as in the prototype. They are the scale factors.

The first scale factor σ/L requires the ratio of size of particle to size of model to be the same in model as in prototype. It could be broadened to include similarity of shape as well, but this would create almost insurmountable experimental problems, and it isn't clear at this stage whether this refinement is necessary in view of other approximations which will be made. It may prove impossible to maintain σ/L in order to satisfy other more important requirements.

The scale factor $m/\rho\sigma^3$ may be changed to the form ρ_p/ρ by replacing m/σ^3 with ρ_p , mass density of the particle, since σ^3 is proportional to volume. This ratio is a measure of the buoyancy force acting on the particle. Since the density of snow particles is so much greater than air density, the buoyancy force is small compared with other forces in snow-drifting phenomena. This scale factor will be neglected.

The ratio V_p/V requires the particle velocity to be scaled in proportion to fluid velocity. This scale factor is significant for its relation to the fluid forces on a snow particle. Using the form conventional in aerodynamics, the resistance force on a particle is given by

$$D_g = C_D \frac{\rho}{2} V_r^2 S_a$$

where

C_D = dimensionless coefficient dependent on the shape of the particle and on the Reynolds number Re

$$Re = \frac{V_r \sigma \rho}{\mu}, \quad \text{Reynolds number}$$

V_r = relative velocity of particle and surrounding air

$$S_a = \pi \left(\frac{\sigma^2}{4} \right), \quad \text{cross sectional area of particle.}$$

Relative velocity V_r is the vectorial difference between velocities, V and V_p , in scalar form

$$\begin{aligned} V_r &= k_3 V - k_4 V_p \\ &= k_4 V_p \left(\frac{k_3}{k_4} \frac{V}{V_p} - 1 \right) \end{aligned} \quad (31)$$

where k_3 and k_4 are factors which depend on the relative direction of V and V_p . When V and V_p are in the same direction, $k_3 = k_4 = 1$. When the scale factor V_p/V and geometric similarity of particle paths are preserved, k_3 and k_4 are the same for model and prototype. V_r is, therefore, proportional to V_p and drag may be expressed in terms of V_p

$$\begin{aligned} D_g &= k_5 C_D \frac{\rho}{2} V_p^2 S_a \\ &= \frac{k_5 \pi}{8} C_D \rho V_p^2 \sigma^2 \end{aligned} \quad (32)$$

where k_5 is another constant which will have the same value in model and prototype.

The last scale factor $V_p \rho \sigma / \mu$ is a form of Reynolds number. V_p may be replaced with V_r in accordance with the above discussion, and the Reynolds number takes the usual form. Insofar as the suspended particle is concerned, the drag coefficient C_D is the only quantity dependent on the Reynolds number and must be selected accordingly. Variation of C_D with Re for spherical objects is well known (see Schlichting, 1955, Fig. 1.5) and will be used as the basis for discussion of snow particles. C_D varies inversely with Re for low values (Stokes's equation range), while at relatively high values C_D is substantially constant. Re for snow particles will generally fall in between these extremes, and no simple function will express the dependence of C_D on Re for more than a limited range.

The variation of C_D with Re will require the mass density of the material used to simulate snow particles to be different from that of prototype snow if the scale factor on particle size is to be maintained. To maintain equal ratio of particle acceleration D_g/m (due to fluid forces) to gravitational acceleration g , the following product must be preserved. On substituting the value for D_g from eq 32, it takes the form

$$\frac{D_g}{mg} = \frac{k_5 \pi C_D \rho V_p^2 \sigma^2}{8 mg} \quad (33)$$

Since m is proportional to $\rho_p \sigma^3$, the product may be written (omitting the constants)

$$\frac{C_D \rho V_p^2}{\rho_p g \sigma} \quad (34)$$

When the Froude number is divided out, there remains

$$\frac{C_D \rho}{\rho_p} \quad (35)$$

This is one form of the scale factor which accounts for the effect of the Reynolds number on particle fluid forces. An alternate form expresses it in terms of particle free-fall velocity V_f . By equating the weight of the particle to its drag in terms of V_f , the equation for C_D is found.

$$C_D = \frac{k_s \rho_p \sigma g}{\rho V_f^2} \quad (36)$$

where k_s is another constant. On substituting this value for C_D into expression 34, an alternate form for the scale factor is found (omitting constants), i. e.,

$$V_p / V_f \quad (37)$$

In view of the scale factor V_p / V_f , V_p / V_f may be replaced by

$$V_f / V \quad (38)$$

This form has certain advantages in performing model experiments. V_f or C_D must be determined for the Reynolds number at which the particle moves. The Reynolds number varies since relative velocity V_r will vary and an average value must be taken. In suspension, a particle will have relative velocity equal to free fall velocity when it is not accelerating and a greater or lesser velocity when under acceleration. Thus the average relative velocity tends to be the same as free fall velocity, and the experimental determination of free fall velocity for the particles to be used as snow simulators automatically selects the correct Reynolds number.

While not specifically included in the above analysis, the wind velocity profile above the snow surface must be considered. Since the fluid forces depend on the local relative velocity of air and snow particles, the velocity field should be properly scaled. Two different cases must be distinguished. The first concerns snowdrift formation around objects exposed to the air stream. Air-flow patterns around objects with sharp edges such as buildings and snow fences remain geometrically similar to relatively small scales (low Reynolds number) and the turbulent velocity components tend to remain proportional to the mean stream velocity. Thus those phases of snow-drifting phenomena dominated by this situation are likely to be properly scaled with regard to the velocity field.

The second case deals with snow movement over flat surfaces and presents greater modeling problems. The extent to which velocity profiles over flat surfaces must be accurately modeled remains to be determined. Since most of the snow movement takes place quite close to the surface, it may be sufficient to model only the lowest layers. Analysis of this problem is hampered by lack of data for the atmosphere as well as by the controlled airstreams of the wind tunnel laboratory. Such information as is available for flow over rough surfaces shows some possibility of proper modeling. Schlichting (1955, eq 20, 32a) gives the following equation for a velocity profile over a rough surface for completely "rough" flow (to be discussed later).

$$V / V_* = 2.5 \log_e (y / k_s) + 8.5 \quad (39)$$

where

V = mean velocity at elevation y

V_* = friction velocity

$$= \sqrt{\tau_0 / \rho}$$

τ_0 = fluid shear stress at the surface

y = elevation or height above the surface

k_s = grain size of sand particles used in the original experiments.

Friction velocity V_* is dependent on particle size, but its evaluation will depend on how a scale model of the atmospheric profile is to be produced in a wind tunnel. There is only a limited amount of data. There is also a fundamental question on whether velocity profiles produced over the almost limitless distances on the earth's surface can be properly scaled in the severely limited size of the wind tunnel test section. The boundary layer (region in which the velocity increases from zero at the surface to the free stream velocity above) has little or no thickness at the beginning of the test section and increases in thickness with distance downstream. There appears to be no similar growth of boundary layer thickness in the atmosphere. In addition to thickening of the boundary layer on a finite length surface, there is also a lowering of surface shear stress with downwind distance. The surface shear stress is important to snow movement near the surface. Whether a boundary layer of constant thickness and shear stress is necessary is not clear but rapidly changing characteristics are certainly not desirable where snow movement over extended flat surfaces is involved.

With a long wind-tunnel test section, experiments may be performed at a downstream location where the layer has reached a desirable height and where rate of growth and change in shear stress are at sufficiently low values. Artificial thickening of the boundary layer may reduce the length of test section needed. If the test section is sufficiently long (with or without artificial thickening), the boundary layers on the floor, walls, and ceiling will eventually meet one another and the uniform conditions of a long tube will be reached. This may yield a suitable constant thickness and constant shear stress boundary layer but this subject requires further exploration. That the shear stress is constant when the uniform conditions of a long tube are reached is shown by the equation for shear stress given in Schlichting (1955, eq 20, 35).

$$\lambda = \frac{1}{[2 \log_{10}(R/k_s) + 1.74]^2} \quad (40)$$

where λ is a coefficient of resistance defined by the equation

$$\tau_0 = \lambda \rho \bar{u}^2 / 8. \quad (41)$$

\bar{u} is the mean velocity of flow through the tube. R is the radius of the tube and k_s is the grain size as introduced above. Since the maximum velocity will occur at the center of the tube, R is the boundary layer thickness. For non-circular shapes, R will be proportional to boundary layer thickness. Preservation of geometric similarity of snow particles in relation to boundary layer thickness or other measures of velocity profile dimensions will be equivalent to keeping R/k_s constant between model and prototype. This will yield the same resistance coefficient as eq 40. In terms of friction velocity

$$V_* = \sqrt{\tau_0 / \rho} \quad (42)$$

$$V_* = \sqrt{\lambda / 8} \bar{u}.$$

This equation has special significance when viewed in relation to eq 39 for velocity profile. On substituting the value for V_* from eq 42

$$V' / \bar{u} = \sqrt{\lambda / 8} [2.5 \log_{10}(y/k_s) + 8.5]. \quad (43)$$

Since at a geometrically similar elevation y , y/k_s will be the same for model and prototype, the velocity profile will be properly scaled.

The saltation phase of snow movement involves complex interactions between snow particles which depend on their elastic or plastic properties. The rebound of a particle

after impact with one or more particles or a boundary surface is an important characteristic. The ratio of velocity of rebound to velocity of impact is defined as the coefficient of restitution e . Since it is desired to preserve the velocity field, the coefficient of restitution should be the same for model and prototype; e becomes another scale factor in the modeling of snow drifting.

The creep phase of snow drifting involves gravitational and fluid forces. When a snow particle at rest is lodged among other snow particles, the weight of the particle produces a moment which opposes the overturning moment produced by air movement. When the aerodynamic moment equals the weight moment, the particle is on the threshold of movement. The velocity at which this occurs is the threshold velocity. Bagnold (1941) has developed the following equation for threshold friction velocity for sand movement. It will have the same form for snow:

$$V_{*t} = k_7 \sqrt{\frac{\rho_p - \rho}{\rho}} g \sigma \quad (44)$$

where k_7 is a constant found to have a value of 0.1 for sand in air and 0.2 for sand in water. Its value is not known for snow. If the ratio ρ_p/ρ has the same value for model and prototype, eq 44 will have the same form as the Froude number and V_{*t} will be proportional to air velocity V . Owing to viscous effects on particle drag, ρ_p/ρ will change in accordance with eq 35.

Equation 44 holds only for "rough" flow, i. e., the condition for which the turbulent boundary layer is close enough to the surface to envelop the particles. As the roughness Reynolds number,

$$Re_r = \frac{V_* k_s \rho}{\mu} = \frac{V_* k_s}{\nu}, \quad (45)$$

becomes smaller, a condition is reached where the laminar sublayer has a thickness comparable to grain size and eq 44 is invalid. A minimum V_{*t} is reached and for smaller particles V_{*t} begins to increase. Dependence of V_{*t} on ρ_p/ρ in eq 44 and the existence of a minimum V_{*t} due to laminar sublayer may make the model V_{*t} higher than that which satisfies the Froude number. Thus atmospheric wind velocities close to atmospheric threshold velocity may be difficult to model. This situation is improved by the fact that once snow movement has started, it will continue at a velocity lower than threshold velocity, called the impact threshold velocity. Feeding the simulating snow from the ceiling of the test section in a wind tunnel experiment will reduce the threshold velocity. The presence of objects causes local regions of higher velocity where snow movement may start at a lower threshold.

Atmospheric threshold velocity for snow movement is sometimes given as 10 mph. Assuming this velocity occurs at an elevation of 6 ft and the snow particle diameter is 0.1 cm, the atmospheric threshold shear velocity may be calculated with eq 39. V_{*t} is found to be 16.4 cm/sec. The roughness Reynolds number Re_r corresponding to these conditions is approximately 12, assuming grain size k_s is the same as particle diameter. Bagnold (1941) reports that the flow around sand particles ceases to be "rough" when Re_r is less than 3.5. Schlichting (1955) shows the flow to be "smooth" when Re_r is less than 5 and "rough" when greater than 70, with a transitional region in between. His data are based on experiments in which particles are not free to move. While there may be differences in the results due to differences in method of measuring particle size, the large difference between Schlichting's experiments and the others is that the surface of loose snow or sand may have been pitted by prior saltation leaving craters larger than particle diameter. This would make the "effective" particle size larger. Regardless of these differences, Re_r for snow in the prototype is not much greater than that for minimum V_{*t} , thus leaving little room for reducing model scale without limiting velocity range because of increasing V_{*t} . If the lower part of the velocity range becomes important, it may be advisable to consider abandoning the requirement of geometric similarity for particle size. This will obviously require change in particle density and may give greater freedom in the selection of material for snow simulation.

In summary, the following scale factors are considered to be significant at this stage of development:

$$\frac{\sigma}{L}, \frac{V_p^2}{g\sigma}, \frac{V_p}{V}, \frac{V_f}{V}, e.$$

In application, the second and third factors may be combined to form a Froude number based on fluid velocity $V^2/g\sigma$. The density of the model particle must be such as to satisfy both σ/L and V_f/V . Consideration should be given to proper scaling of the wind velocity profile, especially near the surface. The discussions of velocity profiles in this paper are based on characteristics obtained when there is no movement of the particles. When the snow particles are in motion, the velocity profile is different. Whether the above modeling criteria are adequate for this situation is a subject for further exploration.

Scale factors based on theoretical analysis of saltation phenomena

The theoretical analysis provides a basis for determining scale factors which apply to saltation phenomena. The assumptions of that analysis will obviously apply here. The surface configuration is that of a flat uniform field of particles. The following analysis begins with the differential equations of motion which apply to both model and prototype. The condition for similarity of trajectories is applied and the scale factors needed to obtain this similarity are found.

$$\ddot{y} + \frac{k_a}{m} \dot{y} + g = 0 \quad (46)$$

$$\ddot{x} + \frac{k_a}{m} \dot{x} = \frac{k_a}{m} k_1 y. \quad (47)$$

If ()_m denotes model variables and we introduce the scale factors:

$$\text{length:} \quad L_s = \frac{L_m}{L} \quad (48)$$

$$\text{velocity:} \quad U_s = \frac{\dot{L}_m}{\dot{L}} \quad (49)$$

$$\text{particle density:} \quad D_s = d_m/d, \quad (50)$$

we may calculate the factor for acceleration quite simply, assuming a steady velocity field:

$$\begin{aligned} \ddot{L}_m &= \frac{d\dot{L}_m}{dt} = \frac{\partial \dot{L}_m}{\partial L_m} \cdot \frac{\partial L_m}{\partial t} = \dot{L}_m \left[\frac{\partial \dot{L}_m}{\partial L_m} \right] \\ &= U_s \dot{L} \left[\frac{\partial \dot{L}_m}{\partial L} \cdot \frac{\partial L}{\partial L} \cdot \frac{\partial L}{\partial L_m} \right] \\ &= U_s \dot{L} \left[U_s \cdot \frac{\partial L}{\partial L} \cdot \frac{1}{L_s} \right] = \frac{U_s^2 \dot{L}}{L_s} \end{aligned} \quad (51)$$

or,

$$\frac{U_s^2}{L_s} = \frac{\dot{L}_m}{L}.$$

The equations of motion are now written for the model, and eq 48, 49, 50 and 51 substituted, giving:

$$\frac{U_s^2}{L_s} \ddot{y} + \frac{k_0 L_s U_s}{m D_s L_s^3} \dot{y} + g = 0 \quad (\text{since } k_0 \sim \sigma)$$

$$\frac{U_s^2}{L_s} \ddot{x} + \frac{k_0 L_s U_s}{m D_s L_s^3} \dot{x} = \frac{k_0 L_s K}{m D_s L_s^3} k_1 L_s y \quad \text{where } K = \frac{k_1 m}{k_1} \quad (52)$$

However, had we selected a different scale factor than L_s for particle size (leaving L_s for dimensions that are large, compared to particle diameter), we would have obtained,

with $\Sigma = \frac{\sigma_m}{\sigma}$,

$$\left(\frac{U_s^2}{L_s}\right) \ddot{y} + \frac{k_0}{m} \left(\frac{U_s}{D_s \Sigma^2}\right) \dot{y} + g = 0 \quad (53)$$

$$\left(\frac{U_s^2}{L_s}\right) \ddot{x} + \frac{k_0}{m} \left(\frac{U_s}{D_s \Sigma^2}\right) \dot{x} = \frac{k_0}{m} \left(\frac{KL_s}{D_s \Sigma^2}\right) k_1 y. \quad (54)$$

The procedure is certainly allowable when (a) particle diameter is much smaller than the critical dimensions of large objects placed on, or restricting, the field, and (b) particles do not influence each other: i.e., collisions between airborne particles are unimportant. Then, for a model particle to behave like a full-scale saltating particle, eq 53 and 54 must reduce to eq 46 and 47 respectively. It is obvious, then, that

$$\frac{U_s^2}{L_s} = 1, \quad (55)$$

$$\frac{U_s}{D_s \Sigma^2} = 1, \quad (56)$$

and

$$\frac{KL_s}{D_s \Sigma^2} = 1 \quad (57)$$

are required of the model.

Before proceeding, we note that the factor k is certainly not an independent parameter. Since

$$k_1 m = \frac{V_{\infty m}}{y_m} = \frac{U_s V_{\infty}}{L_s y^*} = \frac{U_s}{L_s} k_1 \quad \bullet$$

then,

$$\frac{k_1 m}{k_1} = K = \frac{U_s}{L_s}. \quad (58)$$

Therefore, condition (12) reduces to:

$$\frac{U_s L_s}{L_s D_s \Sigma^2} = \frac{U_s}{D_s \Sigma^2} = 1, \text{ or to eq 56.}$$

And, in satisfying eq 55 and 56, we get

$$\frac{L_m}{L} = \left(\frac{L_m}{L} \right)^{1/2} \quad (59)$$

[Written as $V_m^2 / L_m g = V^2 / L g$, eq 59 is recognized as the statement that the Froude number is constant.]

$$\text{and } \frac{\rho_m}{\rho} \left(\frac{\sigma_m}{\sigma} \right)^2 = \left(\frac{L_m}{L} \right)^{1/2} \quad (60)$$

From eq 58, we get:

$$\frac{k_{1m}}{k_1} = \left(\frac{L_m}{L} \right)^{1/2} \left(\frac{L}{L_m} \right) = \left(\frac{L}{L_m} \right)^{1/2} \quad (61)$$

Our modeling must now be subjected to a test for self-consistency. That is, we have required that:

$$\frac{V_{fm}}{V_f} = U_s$$

$$\text{and } \frac{(mg)_m}{mg} = \left(\frac{\rho_m}{\rho} \right) \left(\frac{\sigma_m}{\sigma} \right)^3 = D_s \Sigma^3.$$

But, our basic eq 46 and 47 have been derived using the assumption that

$$\text{Drag} = k_0 u_r,$$

or

$$k_0 V_f = mg$$

or

$$\frac{V_{fm}}{V_f} = \frac{(mg)_m}{mg} \left(\frac{k_0}{k_{0m}} \right) = \frac{(mg)_m}{(mg)} \left(\frac{\sigma}{\sigma_m} \right)$$

which implies that

$$U_s = D_s \Sigma^3 / \Sigma = D_s \Sigma^2$$

i.e.,

$$\frac{U_s}{D_s \Sigma^2} = 1.$$

But this condition has already been met by eq 56.

Therefore, the scale factors are consistent with the physical assumptions.

The model is selected as follows:

- (1) A convenient ratio L_m/L is chosen.
- (2) Free stream and particle velocities must now conform to the ratio

$$\frac{L_m}{L} = \left(\frac{L_m}{L} \right)^{1/2}$$

the boundary layer being adjusted so that

$$\frac{k_{1m}}{k_1} = \left(\frac{L_m}{L} \right)^{1/2}$$

- (3) The particle density and size must be selected so that

$$\frac{\rho_m}{\rho} \left(\frac{\sigma_m}{\sigma} \right)^2 = \left(\frac{L_m}{L} \right)^{1/2}$$

There is some freedom in selecting these properties, but an upper limit is imposed on density by the requirement that the particle possess a reasonable threshold velocity (conforming to the magnitude of other velocities in the problem). The lower limit on density and upper limit on size are obvious.

Our modeling scheme is now virtually complete. We need only consider the boundary conditions: that is, we must require that termination of one trajectory at angle ψ , and velocity v_1 leads to the initiation of another trajectory at angle β_0 and velocity $v_{0'}$, $\psi_{1m} = \psi_1$, $\beta_{0m} = \beta_0$

$$\left(\text{from the condition } \tan \left\{ \begin{array}{c} \psi_m \\ \text{or} \\ \beta_{0m} \end{array} \right\} = \frac{\dot{y}_m}{\dot{x}_m} = \frac{U_s \dot{y}}{U_s \dot{x}} = \tan \left\{ \begin{array}{c} \psi \\ \text{or} \\ \beta_0 \end{array} \right\} \right)$$

and $v_{1m} = U_s v_1$, $v_{0m} = U v_{0'}$. The exact requirement on the ratio of coefficients of restitution, e_m/e , so that these conditions are met is determined by inspection of the interaction equations. These equations show that the variables in question are independent of particle velocity and size; hence the model interaction will satisfy the above conditions only when $e_m/e = 1$.

Selection of model scale and snow simulator properties

The criteria developed in the preceding sections are used to select the requirements to be applied in designing the scale model experiments. At the earliest stage of the project, before these criteria were developed, the search for a suitable snow simulator was based on finding a material which had properties similar to real snow. Lightweight materials seemed to satisfy this requirement and the early tests in the 10 x 20 in. wind tunnel used materials of this type.

In order to select the most effective linear scale for the physical objects to be used in the 3½ by 7 ft wind tunnel, consideration had to be given to the size of the object which can be placed in the tunnel without being seriously affected by the wall and ceiling boundary conditions. Based partly on the fact that the snow drifting studies are concerned with surface flow, it was felt that objects as much as 2 ft high could be used without any serious errors being introduced. Consideration had to be given also to how small the models could be and still achieve meaningful results. If the models and model snow are too small, then the boundary effects and other random effects might be of the same order of magnitude as the desired drifting effects. Another factor considered was the available wind velocity in the wind tunnel. This limits the size of the model snow

particles since, as shown later, the fluid threshold velocity for very small particles is an inverse function of the particle size. After review of the problem, it was decided to use an initial linear scale of 1/10. These conditions would allow the modeling of objects which in reality had heights of as much as 20 ft and widths of up to approximately 40 to 50 ft. Since natural blowing snow on the Greenland Ice Cap has been reported (Gerdel, personal communication) to have a mean grain diameter of 1 mm, the simulating-snow particles must have a mean diameter of 0.1 mm.

The air velocity requirement is determined from the Froude number as follows:

$$\frac{V^2}{gL} = \frac{V_m^2}{gL_m}$$

or for constant g ,

$$\frac{V_m}{V} = \sqrt{\frac{L_m}{L}}$$

Thus for a 1/10 linear scale the velocity must be modeled $\sqrt{1/10}$.

The free settling velocity of the snow-simulator particles must also satisfy the Froude number and must, therefore, have a value $\sqrt{1/10}$ of that of real snow particles. The density of the simulator should satisfy the particle diameter and free settling velocity requirement simultaneously. The coefficient of restitution of the simulator should be the same as that of real snow.

If the velocity profile were modeled as discussed earlier, V_*/V , the ratio of friction velocity (a measure of surface shear stress) to airstream velocity (at geometrically similar elevations), would remain constant as shown by eq 39. For prototype elevation y of 6 ft and snow particle diameter of 0.1 cm as used earlier, eq 39 gives $V_*/V = .037$. It is of interest to compare this with a value estimated for the model experiments. Velocity profile measurements were not made in these experiments but an approximated value may be obtained with the equation for surface friction coefficient over a rough plate (Schlichting, 1955, eq. 21.41):

$$C_f = [2.87 + 1.58 \ln (x/k_s)]^{-2.5} \quad (62)$$

where C_f is the local friction coefficient and x the distance downstream of the leading edge of the plate. C_f is related to V_* , by the equation,

$$V_* = \sqrt{C_f/2V_\infty} \quad (63)$$

where V_∞ is the free stream velocity above the boundary layer. The wind tunnel experiment does not meet the conditions of eq 62 because there is a section of smooth floor upstream of the snow surface, but an approximate value may be obtained. C_f changes slowly with x . Assuming an effective value of 15 ft for x and 0.01 cm for particle size, eq 62 and 63 yield $V_*/V = 0.039$. This is comparable to the value calculated for the atmosphere. For a particle diameter of 0.02 cm, V_*/V becomes 0.042. There arises the question of whether geometric similarity of profiles will be preserved. With equal values of V_*/V , geometric similarity is implied in eq 39 but there is the limitation of boundary-layer depth. No equation for boundary-layer depth appears to be available for the rough plate condition of eq 62. The depth is estimated to be on the order of $\frac{1}{2}$ ft for $x = 15$ ft. The model experiments may, therefore, be expected to give approximate modeling of the velocity profile for a depth corresponding to 5 ft in the atmosphere at $x = 15$ ft. Above this level the model air flow is at constant velocity, while in the atmosphere the velocity continues to increase to a much greater elevation.

Modeling of fluid threshold velocity for snow movement presents the problem discussed earlier with regard to lower limit on rough flow. A minimum roughness Reynolds

number R_τ of 5 will be taken as given by Schlichting (1955) for the beginning of smooth flow. For particle diameter of 0.01 cm, $V_{st} = 70$ cm/sec (eq 45), but for 0.02 cm; $V_{st} = 35$ cm/sec. The free-stream threshold velocity V_t for $V^*/V = 0.042$ and 0.02 cm diam is 19 mph. The equivalent prototype speed would be very high. If this were truly the threshold speed, flow over flat snow surfaces could only be modeled for rather high prototype wind speeds. The wind-tunnel experiments showed that snow movement began at free stream speeds on the order of 11 mph in the flat region upstream of modeled objects when no snow was falling (fluid threshold velocity) and at a lower speed with falling snow (impact threshold velocity). Irregularities in the snow surface probably played an important part by raising the effective grain size.

INVESTIGATION AND SELECTION OF MATERIAL TO BE USED AS SNOW SIMULATORS IN MODEL EXPERIMENTS

Techniques and equipment

Measurement of free-fall velocity.

Large drop chamber with still camera and strobolume: The free-fall velocity is one of the more important characteristics of particles. Equipment and techniques were developed to measure this property. In the first method tried, a test chamber with a cross-sectional area of 10 by 20 in. and a height of 5 ft was used. This chamber had Plexiglas on two adjacent sides and was equipped with a vertical scale. A still camera and a flashing light (strobolume) were placed near the bottom of the chamber so that the light illuminated falling particles at an angle with respect to the camera. The flashing rate of the light was controlled by a high-speed switch. With the shutter of the camera open and the light flashing, particles were dropped in the test chamber. This produced a series of successive images as the particles fell past the camera. Since the flashing rate of the light was known and the distance traveled was measured on the vertical scale, the free-fall velocity of the particles could be calculated. In order to insure that free-fall velocity had been reached, the fall path of the particle was about 5 ft long before it entered the camera's view. The major deficiency of this method is that one cannot be certain that two successive images on the photographic plate were made by the same falling particle.

Two-camera technique: Two still cameras and a time-delay mechanism were used with the drop chamber just described. The two cameras were placed at different heights outside the chamber with the lower camera triggered a split second after the upper one. A millisecond timer measured the delay between the two exposures. The delay was varied until it was possible to observe the same particle in the photos taken by the two cameras. Although the basic procedure was sound, this method was not used extensively after a high-speed motion picture camera became available.

Drop chamber and high-speed motion picture camera: A drop chamber was constructed which provided back lighting of the falling particles by a 150 w light source placed behind a frosted glass plate (Fig. 12). The falling particles were photographed by a high-speed motion picture camera, * at approximately 600 frames per sec. As used in previous techniques, a strobolume illuminated the camera's field at a rate of 50 flashes per sec. In this way the flashing light would appear on the film about once every 12 frames. This method yielded very satisfactory results and was used to determine the fall velocity of snow grains. A later refinement to this method was made by using a neon light bulb in the field of view. The film speed was fast enough to detect the on and off periods of the light bulb when an ordinary 60-cycle a-c current was used for illumination. This provided a much better timing mechanism than had been used previously.

Density measurement. Since the density of a small particle is an important factor in its terminal fall velocity, attempts were made to develop a method for measuring the densities of the substances which might be suitable for a model snow. It was found that for many non-crystalline or non-uniform substances like cork, wood, fly ash, etc. the densities reported in the literature varied greatly depending on the conditions under which they were measured. A simple experiment showed that cork particles which had

*Bell and Howell Traid 70.



Figure 12. Drop chamber showing the Bell and Howell high-speed camera in position.

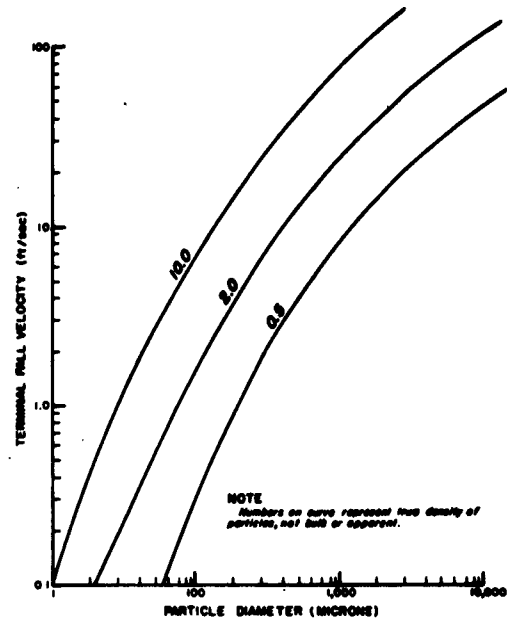


Figure 13. Terminal velocities of spherical particles of different density settling in air at 70F under the action of gravity. (Extracted from Perry, 1950, p. 1021).

been reduced to powder would not float on water (neglecting surface tension effects) although the density of cork is reported to be 0.207 by Hodgman (1952). Three approaches to the density measurement problem were undertaken.

Weight and volume technique: The first approach was an attempt to refine the standard weight-per-unit-volume technique. Ten-milliliter samples of several sizes of test materials were vibrated until they appeared to be well settled (i. e., little measurable reduction of volume seemed obtainable). Using the approach described by Dalla Valle (1948) to estimate the percentage of voids, the volume of the test solids was calculated. The samples were then weighed on a microbalance and the density was computed by the elementary relationship:

$$\text{density} = \text{mass/volume.}$$

The uncertainties of this method are quite apparent. The equations mentioned in Dalla Valle's method involve certain assumptions of sphericity and "closeness" of packing. Since most of the test materials contain unspherical particles, some errors in the results are to be expected. When materials of known densities were used in this method the results appeared to be too low, probably due to incomplete packing of the sample.

Air suspension technique: Another method used to calculate densities involved mounting a large glass tube in a vertical position. Test particles dropped in the tube were held in mid-tube by forcing a stream of air up through the tube. The velocity of the air was measured by a flowrator. The velocity required to exactly balance the particles represents a measure of the terminal velocity of the particles. The densities were then calculated using Stokes's law.

V_{ft} = terminal settling velocity of particle

ρ_p = density of particle

ρ = density of fluid

r = radius of particle (assumed to be spherical)

g = gravity

μ = viscosity of fluid.

An error is introduced in the application of this equation to the problem since the actual curves become non-linear for particle diameters greater than 50 to 75 μ (Fig. 13). Thus in the intermediate range of diameters between 50 μ and a few thousand microns neither Stokes's law nor the ordinary laws of free-falling bodies are completely valid. For this reason it was decided to measure the terminal fall velocity of the materials selected for possible use as snow simulators.

Two-liquid technique: From among the samples, pairs of particles were selected so that each pair was closely matched in size and shape. One of each pair was dropped into a column of distilled water and its time of fall (or rise for light materials) was measured through a known distance. The other particle was dropped into a column of another liquid of known density (carbon tetrachloride was used in these experiments), and its time of fall was measured through an equal distance. The ratio of the two time periods was the value sought. A graph was developed by measuring this ratio for a number of substances of known density. This method was abandoned because of a revised theoretical approach to the entire snow material selection problem, which is discussed in another section.

Free-fall velocity of snow particles

A literature search for the mean terminal fall velocity of natural snow did not yield any conclusive value for the type of snow usually found on the Greenland Ice Cap. It was therefore decided to set up an experiment to determine this value for natural blowing snow as well as for all the proposed model materials. It was felt that a photographic technique would yield the best results in this type of study. Several arrangements involving a drop chamber and photographic equipment were tried before satisfactory results were obtained using a high-speed motion picture camera.

The experimental phase of this work was performed by New York University scientists at SIPRE's cold laboratory in Wilmette, Illinois. A sample of snow from the Greenland Ice Cap was used. The test was carried out in the 22F cold room using a Fastax camera. The basic procedure is described above although some modifications in camera speed and setting were made. Several rolls of high-speed motion pictures were taken of falling snow particles between 1.0 and 1.4 mm in diameter. On the resulting films 20 representative particles were tracked for 1/40 sec (50 frames). There appeared to be great uniformity in the size and velocity of the snow grains. The results are shown in Table I. The mean vertical velocity computed from these measurements was 209 cm/sec.

Physical properties of particulates to be used as snow simulators

Low-density materials. In the early stage of the investigations a number of low-density materials were selected for testing as potential snow simulating materials and also to determine, if possible, whether the test procedures were adequate. The results of these tests on a group of materials are presented in Table II. None of the materials tested were considered to be suitable.

During the course of these tests, it became apparent that, for some of the non-crystalline materials, there was a relationship between particle size and density and that this phenomenon should be investigated before further consideration be given to such materials. Physical inspection showed undesirable characteristics such as the inability to remain free flowing and extreme variability in physical properties. The remainder of the materials were tested for free-falling velocity and density by one or more of the methods described previously (Table II). It was concluded that further investigation should be made on these and other possible materials.

A RoTap Siever and a set of U. S. Standard Sieves were used to prepare test samples of cork particles. A sample of ground cork was sieved until there was no appreciable change in the quantity of particles remaining on each of the sieves. The samples were then removed from the sieves and each sample was then resieved briefly through the next larger sieve in the series. This double sieving was done on the assumption that the non-spherical particles may go through the sieve endwise over a long sieving period while a short sieving period will retain some of the larger ones. The particles

Table I. Fall of 20 snow grains in 1/40 sec.

Particle no.	Vertical distance (cm)	Particle no.	Vertical distance (cm)
1	4.36	11	6.43
2	5.23	12	5.67
3	4.17	13	4.56
4	5.76	14	5.56
5	5.80	15	5.88
6	5.44	16	5.23
7	4.72	17	5.28
8	5.04	18	6.20
9	5.72	19	5.56
10	4.36	20	4.88

Table II. Physical properties of materials originally proposed as snow simulators.

Name	Bulk density (lb/ft ³)*	Exp density (g/cm ³) †	Size (mm)**	Free fall velocity (cm/sec) ††
Vermiculite	10	0.16	0.2	18.5
Styrofoam	1.8	0.03	4.0	28.7
Balsawood sawdust	7.49-12.49	0.12	0.3	26.6
Mica	165	2.7	0.1	
Polystyrene	2	0.03		
Flocking (cellulose rayon)	12	0.20	1.0 (length)	13.3
Cork	12.92	0.38	0.4	15.5
Foam rubber	6	0.1		
Fly ash	35 (variable)	0.5	0.1	

* Taken from literature.

† Measured by weight and volume technique.

** Mean size as determined by a set of standard sieves.

†† Measured by the still camera and strobolum method.

which remained on the larger sieve after the second sieving were assumed to have approximately the dimension of the larger sieve and these were used in the density testing. The samples were tested by both the weight-and-volume method and the air-suspension method. The results are shown in Table III and Figure 14. The approach of the density of the smaller particles toward higher values agrees with the observation of cork powder in water mentioned previously.

High-density materials. The following characteristics were taken as representative of natural blowing-snow particles on the Greenland Ice Cap.

Diameter = 0.1 cm (Gerdel, personal communication)
Free-fall velocity = 209 cm/sec (from experiments reported above)
Coefficient of restitution = 0.33 (from experiments reported below)

Applying the modeling criteria to a linear scale of 1/10, the following desired properties of the snow simulator are found.

Diameter = 0.01 cm
Free-fall velocity = 66 cm/sec
Coefficient of restitution = 0.33.

In order to satisfy the requirement on size and free-fall velocity, the simulator material must have a density greater than that of snow particles. A guide to the approximate density required, which is needed in the preliminary selection of materials, can be obtained by applying the Stokes's law form of free-fall velocity equation for spheres. This equation gives a density of 2.1 g/cm³ for the above simulator properties. Materials having density near this value were selected.

Free-fall velocity: The use of the high-speed motion picture technique described previously made it possible to obtain reliable values for free-fall velocity. A series of tests showed that the camera speed was sufficiently constant so that no timing device was necessary. The limits of variability of the camera were found to be from 211 to 221 frames per second after the initial acceleration period of 4/5 sec. Since these deviations produced a maximum error of only 2.3%, the assumption that the camera ran at an average of 216 frames per second was considered satisfactory.

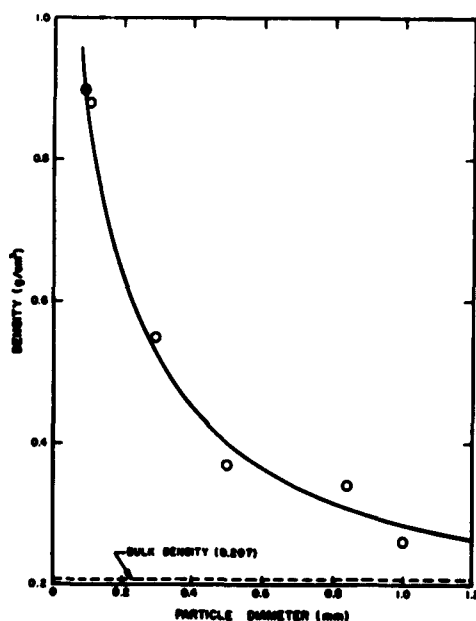


Figure 14. Relationship between particle diameter and particle density for cork.

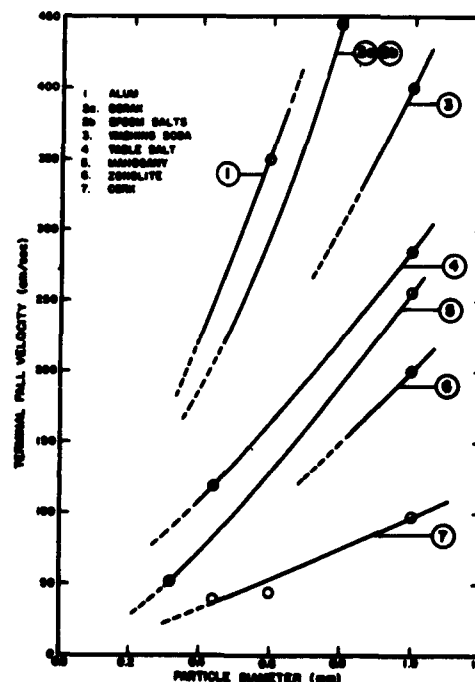


Figure 15. Relationship between particle diameter and free-fall velocity for larger sized particles.

SCALE MODEL STUDIES ON SNOW DRIFTING

31

Table III. Density tests on cork particles.

U. S. Standard Sieve no.	Size (μ)	Weight and vol. method (g/cm ³)	Air suspension method (g/cm ³)	Mean (g/cm ³)
	powder			1.0 (*)
170	88	0.87	0.93	0.90
140	105	0.83	0.93	0.88
50	297	0.51	0.59	0.55
35	500	0.35	0.39	0.37
20	840	0.30	0.38	0.34
18	1000	0.20	0.32	0.26
	bulk			0.207 (†)

* Powdered cork was observed to sink in water.

† Reported by Hodgman (1952).

Table IV. Terminal velocity tests using high-speed motion picture camera.

Material	Chemical formula	Size (mm)	Density* (g/cm ³)	Terminal velocity (cm/sec)
Alum	$\text{KAl} \cdot (\text{SO}_4)_2 \cdot 12\text{H}_2\text{O}$	0.6	1.75	350
		0.1		33
Borax	$\text{Na}_2 \text{B}_4\text{O}_7 \cdot 10\text{H}_2\text{O}$	0.8	1.73	445
		0.1		60
Epsom salts	$\text{M}_g \text{SO}_4 \cdot 7\text{H}_2\text{O}$	0.8	1.64	445
		0.1		50
Washing soda	$\text{Na}_2 \text{CO}_3 \cdot 10 \text{H}_2\text{O}$	1.0	1.44	400
Table salt	$\text{Na}_2 \text{Cl}$	1.0	2.17	285
		0.44		120
Mahogany		1.0		255
		0.32		53
Zonolite		1.0		200
Cork		1.0		98
		0.6		44
		0.44		41
		0.2		30
Magnesium carbonate	$\text{M}_g \text{CO}_3 \cdot 5\text{H}_2\text{O}$	0.2	1.69-.73	68

* Taken from Hodgman (1952).

The first attempts to use the camera produced reliable values only for the larger (0.5 to 1.0 mm) particles. The 0.1 mm particles were not identifiable on the film. However, this method was used on a number of test materials and the results were extrapolated in an attempt to narrow the investigation to a few materials (Table IV, Fig. 15). By means of an auxiliary closeup lens and a refined focusing technique, it later became possible to identify the particles in the 0.1 mm size. The results of the free-fall velocity tests are shown in Figure 16 and Table IV.

Coefficient of restitution: Saltation is also one of the important factors in the occurrence of blowing snow as shown by the theoretical study presented above. It is necessary to consider in detail the rebounding of snow grains when they strike the snow surface. A snow grain which strikes the surface during the saltation process cannot rebound with more kinetic energy than when it struck (barring outside influences). In practice most materials will rebound with some lesser amount of kinetic energy. Since the mass of the particle remains unchanged, this loss of kinetic energy can be expressed by the ratio of the rebound velocity to the striking velocity. This ratio is known as the coefficient of restitution (see p. 6). According to Eshbach (1936) this factor depends only on the materials involved in the impact and is not affected by their size or shape, etc. The coefficient of restitution is considered to be an important factor in the saltation process. For this reason it was decided to attempt to measure the values of the coefficient for snow grains and some of the potential model-snow materials.

The coefficient of restitution was measured by use of the drop chamber and the high-speed camera to photograph small pieces of the test material dropping on to a flat surface of the same material. The falling and rebounding velocities of the material were calculated and the ratio of the two gave the coefficient of restitution. These tests were made on four materials, two of which have known values for the coefficient:

- a. Steel - 3/32 in. carbon steel bearing balls dropped on a steel plate.
- b. Glass - 1.0 mm glass beads dropped on 1/4 in. plate glass.
- c. Borax - small crystals of borax (approx. 2 mm) dropped on a large borax crystal oriented so that a flat surface was normal to the drop line.
- d. Ice grains - small pieces of ice (1.0 mm) prepared by freezing drops of water and dropped on a block of ice.

The entire experiment on ice grains was conducted in a refrigerated room in which the air temperature was -21°C. The results of these tests are given in Table V. The discrepancy between the published and observed values for steel may be due to difference in the type of steel used. The type of steel used to obtain the published value is not cited in the literature.

Threshold velocity: A study of the relationship between particle size, particle density, and threshold velocity was undertaken in the pilot wind tunnel, which has a test section of 10 in. by 20 in. by 8 ft. In the first test a number of materials of different densities were prepared to a uniform particle size of approximately 0.5 mm. Each of these materials was exposed in the pilot tunnel while the velocity of the wind was gradually increased to the threshold value. The results (Fig. 17) demonstrate, as would be expected, that the threshold velocity increases with increasing particle density. In a second test, uniform samples of cork were prepared in approximately the following sizes: 0.1, 0.3, 0.5, 0.8, and 1.0 mm in diameter. Again, samples of each were exposed in the wind tunnel and the threshold velocity was determined for each size. The results (Fig. 18) show that the threshold velocity diminished with decrease in particle diameter down to a minimum at approximately 0.8 mm diameter and then increases. The relationship between threshold velocity and particle diameter appears to be associated with the viscous surface layer of air into which very small particles sink and are undisturbed by moderate winds. However, the thickness of this boundary layer diminishes with increasing velocity and eventually exposes small protuberances and ripples to the effect of higher winds.

Selection of a snow simulator from the materials tested:

From the results of these studies it was decided to use commercial borax ($\text{Na}_2\text{B}_4\text{O}_7 \cdot 10\text{H}_2\text{O}$) as the snow simulator in the first series of tests in the large wind tunnel. The borax appeared to more nearly approach the requirements for a modeled snow than any of the other materials tested; in addition, it was commercially available in large quantities, economical, and easily handled. The particle size distribution of a sample of the borax used in the wind tunnel is shown in Table VI. The mean size of the particles was larger than desired, but the cost of obtaining it in 0.1 mm size was prohibitive. The distribution characteristics, however, compare favorably with those for snow grains given by Dfunin (1956).

A photomicrograph of the borax crystals (Fig. 19) shows them to be quite similar to old snow grains.

WIND TUNNEL MODIFICATION

Two of the New York University wind tunnels were used in various stages of this project. The 10 x 20 in. wind tunnel was used to study snow simulating materials, make preliminary snow-drifting experiments, and test proposed design changes for the $3\frac{1}{2}$ x 7 ft wind tunnel where the final snow-drifting experiments were made.

The 10 x 20 in. wind tunnel has a test section 10 in. wide, 20 in. high, and 8 ft long in the direction of air movement. One wall and the ceiling are made of glass. The wind tunnel draws air from and exhausts to the laboratory atmosphere. The particles which are drawn out of the test section are collected in a cloth bag which covers the exhaust.

The $3\frac{1}{2}$ x 7 ft wind tunnel has a test section $3\frac{1}{2}$ ft high, and 7 ft wide and a usable length of 30 ft. The general layout of the test section is shown in Figure 20. The air supply is taken from within the laboratory building and first passes through various air straightening devices before it reached the test section. The air is drawn through the wind

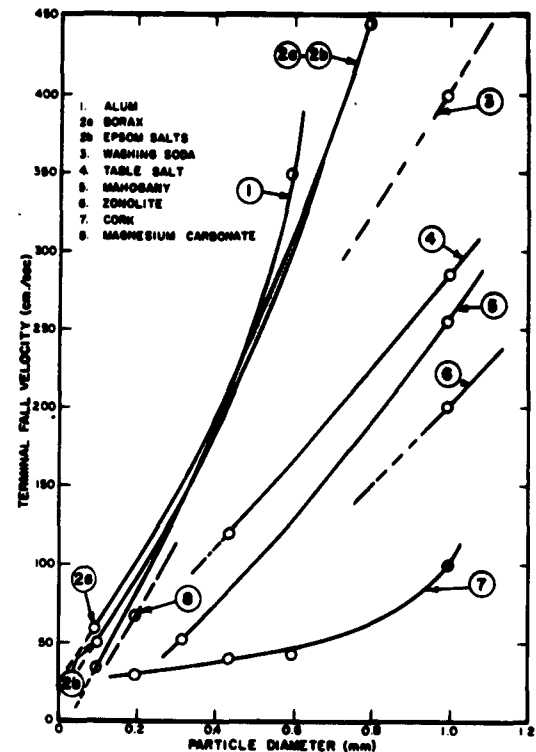


Figure 16. Relationship between particle diameter and free-fall velocity for all particles measured.

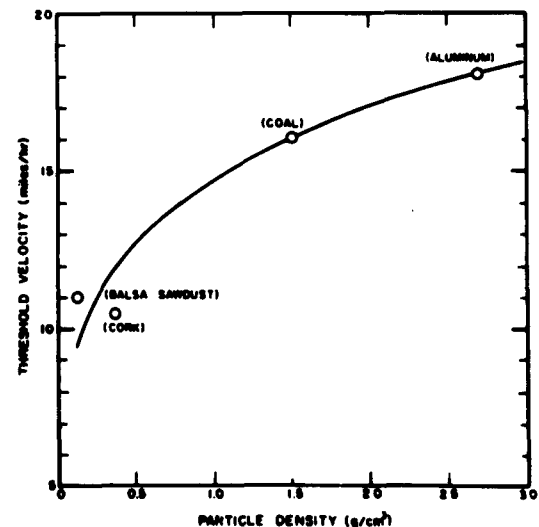


Figure 17. Relationship between particle density and fluid threshold velocity.

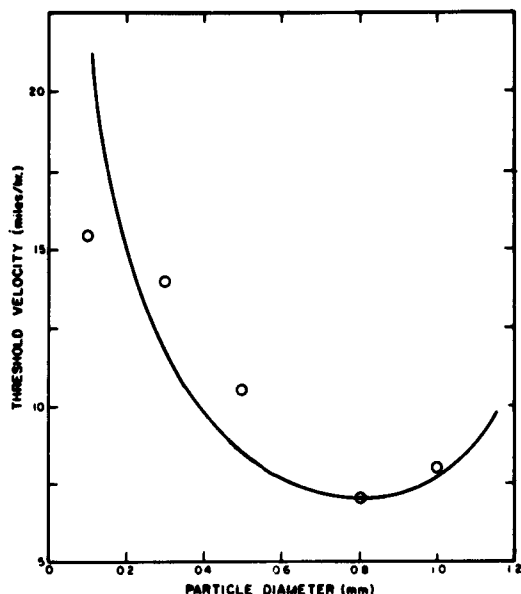


Figure 18. Relationship between particle diameter and fluid threshold velocity for cork.



Figure 19. Photomicrograph of 0.1 mm borax crystals (enlargement 25x).

Table V. Coefficient of restitution measurements.

Material	Published value*	Exp value
Steel	0.55	0.66
Glass	0.95	0.95
Borax		0.55
Ice grains		0.33

*Data taken from Eshbach (1936)

Table VI. Size distribution of borax used in the tunnel tests.

Sieve no.	Material retained			
	Sample A		Sample B	
	Vol. (cm ³)	% by vol.	Weight (g)	% by weight
18 (1000 μ)	0	0	0	0
20 (840 μ)	trace	<0.1	0	0
35 (500 μ)	trace	<0.1	0	0
50 (297 μ)	130	8.0	59.4	11.2
140 (105 μ)	1415	87.0	450.85	84.9
170 (88 μ)	40	2.5	18.70	3.5
greater than 170	40	2.5	2.15	0.4

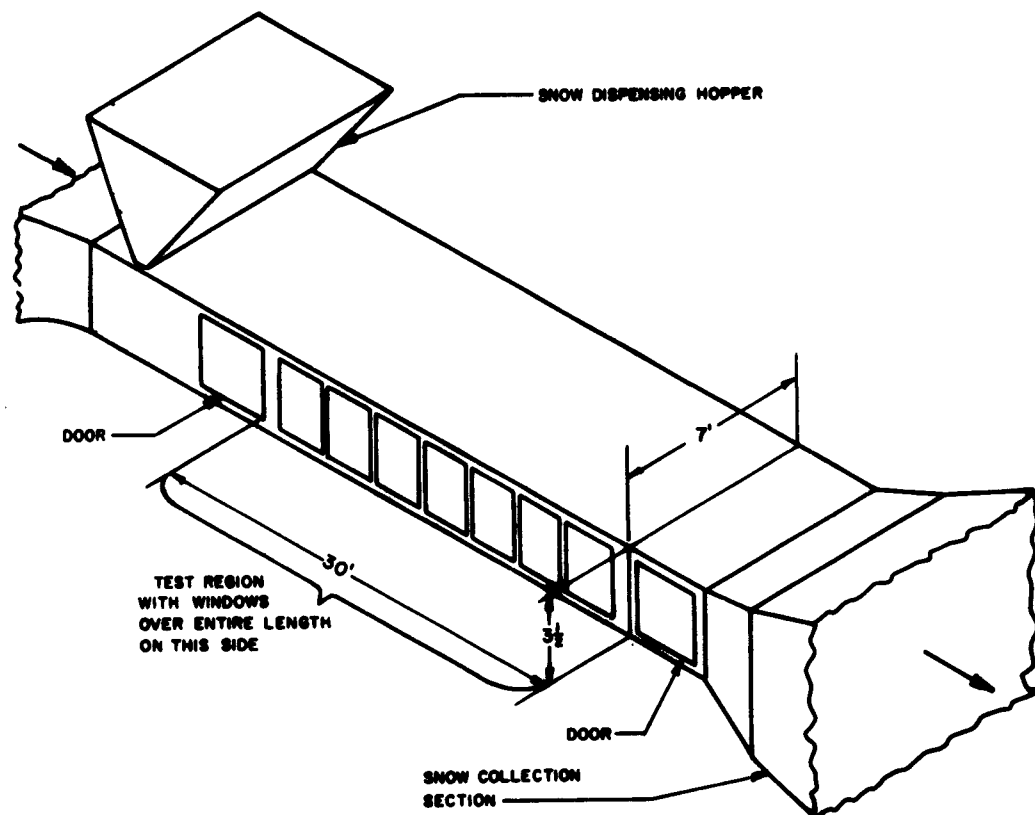


Figure 20. Sketch of test section of New York University $3\frac{1}{2} \times 7$ ft wind tunnel.

tunnel by a variable speed exhaust fan located downstream of the test section and is exhausted through the roof.

The major modification made to the wind tunnel for the snow-drifting experiments was the installation of a hopper to introduce the snow material through the ceiling at the upstream end of the test section. This served to produce the effect of falling snow which is one of the features of the snow environment on the Greenland Ice Cap. High velocity alone will not always cause blowing snow on the Ice Cap (e. g., Hamilton, 1958). The falling snow appears to loosen particles previously deposited on the surface and to initiate saltation at a lower wind speed than would otherwise be required to start movement.

The hopper was designed to handle powdered borax which had been selected for the snow simulator. A small hopper was first tested in the 10 x 20 in. wind tunnel. Clogging and bridging of the borax created difficulties which required modification of the original design. When the first series of experiments was conducted it became evident that further modifications would be necessary for efficient handling of the several tons of borax used in the experiments. During the course of an experiment, the moving snow material collected in an enlarged portion of the wind tunnel downstream of the test section ahead of the exhaust fan. It was periodically removed and transferred to the hopper.

SCALE MODEL STUDIES ON SNOW DRIFTING

SCALE MODEL EXPERIMENTS ON SNOW DRIFTING

CHARACTERISTICS OF VARIOUS STRUCTURES

The final scale model experiments were conducted in the $3\frac{1}{2} \times 7$ ft wind tunnel described earlier. No attempt was made to scale the velocity profile in these experiments. The modeled objects were placed approximately 15 ft downstream of the location where the simulating snow was dropped into the airstream from the hopper. Before an experiment was started, the floor of the test section was covered with a layer of simulating snow which extended about 13 ft upstream of the modeled objects. Upstream of the snow there was 7 ft of bare test section floor surface which joins the wind tunnel contraction cone.

In the initial tests it was not possible to make any exact measurements of the snow drifts around the various models. However, an excellent set of photographs were obtained for all the tests; and most of the tests were also recorded in time-lapse motion pictures. The time-lapse pictures were taken every $1\frac{1}{2}$ sec, so that a period of 1 hr and 40 min could be recorded on a 100-ft roll of film. Inspection of the photographs and the motion pictures, plus visual observation during the tests, produced the qualitative results presented in this report. All of the tests were run at a tunnel velocity of 19 ft/sec (13 mph) which corresponds to an atmospheric velocity of 41 mph. At this tunnel speed the borax particles seemed to be just above the fluid threshold velocity. Only a few borax particles were in motion when the material was not falling from the overhead hopper, while the whole tunnel was filled with blowing borax when the hopper was feeding the windstream. During this latter process saltation was very well developed and surface creep was also very active, as shown in the time-lapse motion picture. Five different model situations were studied and are described below.

Clements-panel buildings oriented crosswind: Four models of Clements-panel buildings, frequently used in Arctic locations, were constructed to represent a prototype structure 60 ft long, 25 ft wide, and 10 ft high. They were erected on pilings which represented a 5 ft elevation from the surface of the snow*. This first building was placed about 15 ft (scaled) downwind of the slot where the snow was entering the windstream. The structures were oriented with their long axes normal to the wind and with the distance between the buildings equivalent to a scaled 25 ft. Figures 21 through 28 show this test at various stages during drift accumulation.

The snow was introduced into the windstream for a period of 3 hr. This "snow-storm" was approximately equal to all the blowing snowstorms occurring during 1 yr in certain areas on the Greenland Ice Cap. After this phase, the test was continued for another 2 hr with only the wind blowing. This later phase represents a period of high wind without precipitation in Greenland. Such winds cause erosion of the surface with loss of snow at one location and deposition at another. This phase of the tests was undertaken to determine the interrelationship between erosion and building or structure design. During the first 3 hr the structures became almost completely drifted over with snow. However, during the later part of the test, a considerable amount of the snow was removed from around the structures by erosion. The photographs give a good qualitative illustration of the processes during the accumulation and erosion periods.

Outstanding in Figure 21 is the stream of snow blowing off the roof of the upwind structure. The stream is striking the side of the next building and most of the snow is falling into the space between the buildings. With this layout the open space between buildings could be expected to become drifted in with snow very rapidly. In Figure 22 the roof of building 1 is well covered with snow while the roofs of the following structures are entirely clear. This is most likely due to a combination of two factors. The alteration in the wind velocity pattern due to the blocking effect of the first structure and the consequent change in the capacity of the air to support the mass of snow causes significant amounts of snow to be deposited in front of and on the roof of the first structure. The second structure is in the wake of the first and the air passing immediately over it is unsaturated with respect to its capacity to hold snow so that very little snow accumulates on the building and in the space between buildings 1 and 2. This is substantiated

* Throughout this section of this report, the word snow is used to signify both real snow and the model snow (borax). It is not felt that any confusion will arise in the meaning whenever it is used.

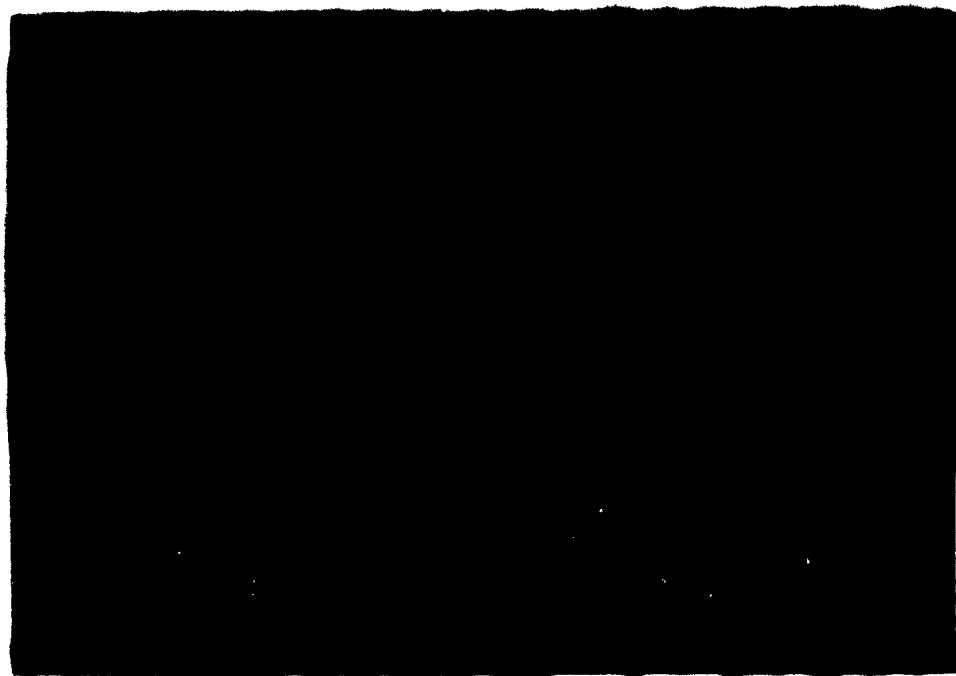


Figure 21. Clements panel buildings nos. 2 and 3 (numbered from upwind) oriented crosswind, $\frac{1}{2}$ hr after start of test. Wind velocity from left to right.



Figure 22. Clements panel buildings nos. 1, 2, and 3 oriented crosswind, 1 hr after start of test.



Figure 23. Side view of buildings nos. 1, 2, and 3 at the same time as shown in Figure 22.



Figure 24. Clements panel buildings nos. 1, 2, and 3 oriented crosswind, 3 hr after start of test.



Figure 25. Clements panel buildings nos. 3 and 4 oriented crosswind, 3 hr after start of test.



Figure 26. Clements panel buildings nos. 1, 2, and 3 oriented crosswind, $3\frac{1}{2}$ hr after start of test, $\frac{1}{2}$ hr after start of erosion.

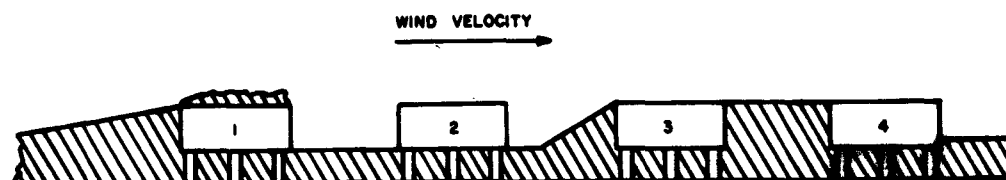


Figure 27. Schematic view of drift pattern after 3 hr of snow deposition.

by Figure 23 which clearly shows the eddy pattern over the first building. The free stream pattern lowers after passing the first building so that it sweeps the roof of the next building clear.

Figures 24 and 25 show the buildings at the end of the snow-storm period. It can be seen (Fig. 27) that the final accumulation pattern is related to the events which occurred during the testing period. Building 1 is completely inundated in front and the roof is still covered; building 2 and the space between 1 and 2 remain relatively clear. The space between buildings 2 and 3 contains a drift with a very sharp upwind slope. This agrees with the flow pattern shown in Figures 21 and 23. The space between buildings 3 and 4 has been completely filled, and the roofs of buildings 2, 3 and 4 have remained clear. The results of this phase of the test indicate that the spacing between buildings may have been insufficient to permit high velocity flow during the accumulation period. The build-up of snow around the buildings shown in Figure 26 appears to be due in part to the coalescence of drifts produced by each building. Roots and Swinbank (1955) reported such coalescence of drifts at Maudheim in the Antarctic where spacing between buildings was inadequate.

After the erosion phase began (Fig. 26), the roof of building 1 started to clear and the space between buildings 1 and 2 started to fill up. This is probably explained by the fact that surface creep is a very important factor in this phase. After 2 hr of erosion (Fig. 28), the roof of building 1 is cleared and the entire drift pattern is decreasing as the strong wind constantly removes small amounts of snow from the test area.

Clements panel buildings oriented downwind: The same four buildings used in the first test were also tested with their major axes parallel to the windstream. The separation between each building again represented a scaled distance of 25 ft. This arrangement was subjected to a snow deposition period of 3 hr with all other conditions maintained similar to the first test. Inspection of the photographs (Fig. 29, 30) shows that the leading edge of the roofs of the upwind buildings became snow-covered, while

in the central area the roofs were essentially clear. This was a consistent feature of the tests with buildings erected with the long axis parallel to the wind flow. The orientation of the buildings with their long axes parallel to the wind appeared to induce channelizing of wind flow and increase velocity, resulting in less deposition against the side walls of the buildings after the clear under-space was saturated. It is not known whether this channelizing and self-clearing action would prevail on the Greenland Ice Cap where winds, although predominantly from one direction, can shift through 20 deg during the progress of a major storm. In addition, under natural conditions storm winds accompanied by falling and drifting snow may be from a direction 45 deg divergent from clear weather winds. Drifts accumulated between buildings by wind from one direction may be protected from erosion by the buildings when the wind shifts a few degrees.

Elevated radar type building: A model was constructed (Fig. 31, 32) to represent a building 50 ft wide, 60 ft long, and 10 ft high set on columns which gave it a 10-ft elevation above the snow surface. This model was exposed to 3 hr of snow deposition. The most significant feature of this test was that the blowing snowstorm initially caused erosion under the model. This erosion was great enough to remove the entire layer of snow under the model and reveal the floor beneath. This test was repeated with a much deeper layer of snow under the model. Again erosion occurred to such an extent that the stability of the model was threatened.

This same model was modified so that it was supported on a buried foundation or crib (Fig. 33). The model foundation used was a rectangular frame of 2 by 4 in. beams buried flush with the snow surface. Erosion began at the start of the test but quickly reached an equilibrium pattern shown by the dashed line (Fig. 33). At no time was the stability of the structure threatened. After equilibrium was reached, drifting proceeded in the usual manner (Fig. 34). As a corollary to this experiment, a model was buried so that its flat roof was flush with the snow surface. No drift snow accumulated on the roof or in the vicinity of this structure. This approach to the problem would be ideal except that many structures (particularly radar buildings) must have above-surface exposed sections to house electronic detection equipment.

Snow fence models: Models of two different types of snow fences were constructed and tested briefly to see if the $3\frac{1}{2}$ by 7 ft tunnel produced a pattern which was comparable with observed natural conditions. The first of these was a 10:1 scale model of one of the drift fences used by the Union Pacific Railroad. This fence was tested in both a vertical (Fig. 35) and a 60° position (Fig. 36). The other fence tested was a 10:1 model of a paper strip fence (Fig. 37, 38) previously tested on the Greenland Ice Cap and discussed by Gerdel (1960). The accumulation of snow by this fence during the test period (3 hr) agrees in a qualitative sense with the pattern shown by Gerdel. The accumulation by the Union Pacific type fence also agreed with the classical atmospheric drift pattern for both angles of inclination. Differentiation between the characteristics of the two different angles was not attempted at this time.

In another test the Union Pacific type fence was set up at a 90° angle with the V of the angle pointing upwind (Fig. 39). This arrangement produced a very long area of minimum accumulation downwind of the fence (Fig. 40). The length of this area was equal to approximately 25 times the height of the fence. Since the fence represented an actual height of 8 ft, this clear area represents an extent of about 200 ft. This fence shape might prove very effective in keeping a moderate-sized area free from drifting. Further testing of this arrangement appears to be very desirable.

Fuel storage tanks: In the last test a number of cylindrical tanks were prepared which represented POL storage tanks with a height of 10 ft and a diameter of $9\frac{1}{2}$ ft (Fig. 41, 42). These were subjected to snow deposition in the same way as the other models. These tanks developed the same trough pattern on their downwind side as did the V-shaped fence. The base of each tank remained clear for a period of time, but when the snow near the tanks became high enough, it began to slide down into the empty space, eventually filling it up.



Figure 28. Clements panel buildings nos. 1, 2, and 3 oriented crosswind, 5 hr after start of tests, 2 hr after start of erosion.

The borax has a lesser angle of repose and less coherence than snow; consequently it may be presumed that the vortex-produced clearing around each tank may have been less deep in the wind tunnel test than it would be under natural conditions unless the natural snow is sufficiently hard to resist erosion.

FUTURE WORK

Further investigation in this field of synthesized blowing snow environments is needed. The theoretical study of the blowing snow process should be given more emphasis. The correlation between the theoretical work and the actual movement of synthetic snow particles should be investigated in more detail.

Much further work also can be done on the 10:1 scale testing. All tests should be repeated with emphasis on the quantitative aspects of the drifts. In addition many different types of snow fences and other structures should be tested.

A program should be initiated to develop a synthetic snow material which could be used for a much smaller scale, e. g. 50:1. This would greatly increase the number and size of models which could be studied in the wind tunnel and permit investigation on the interaction between units in large installations composed of many buildings and different types of structures.

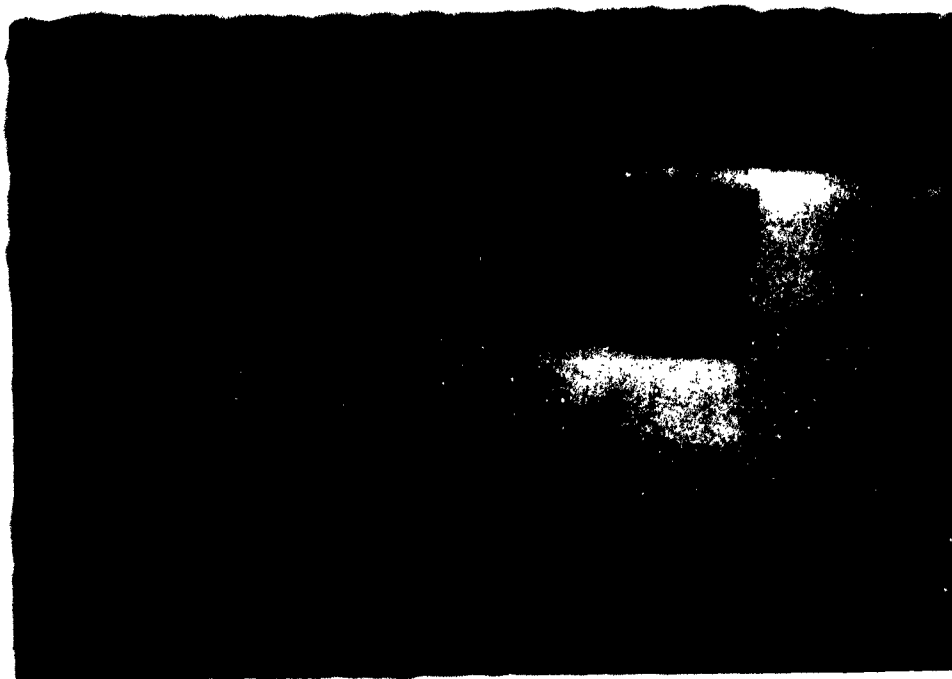


Figure 29. Clements panel buildings oriented with the wind, 2 hr after start of test, looking downwind.

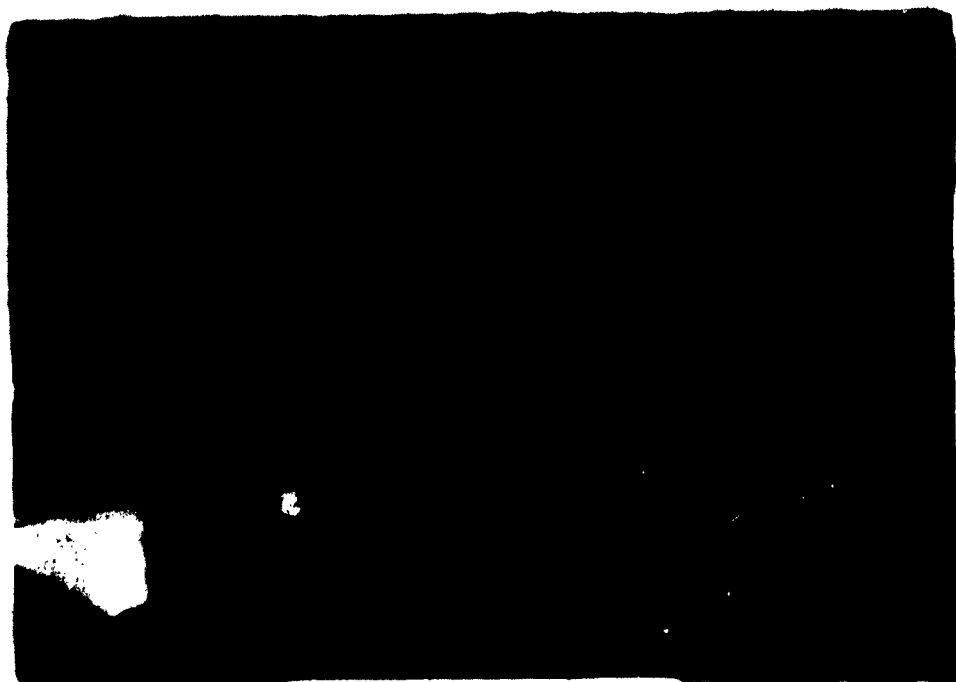


Figure 30. Clements panel buildings oriented with the wind, 2 hr after start of test. Side view.



Figure 31. Radar type building, 1 hr after start of test.

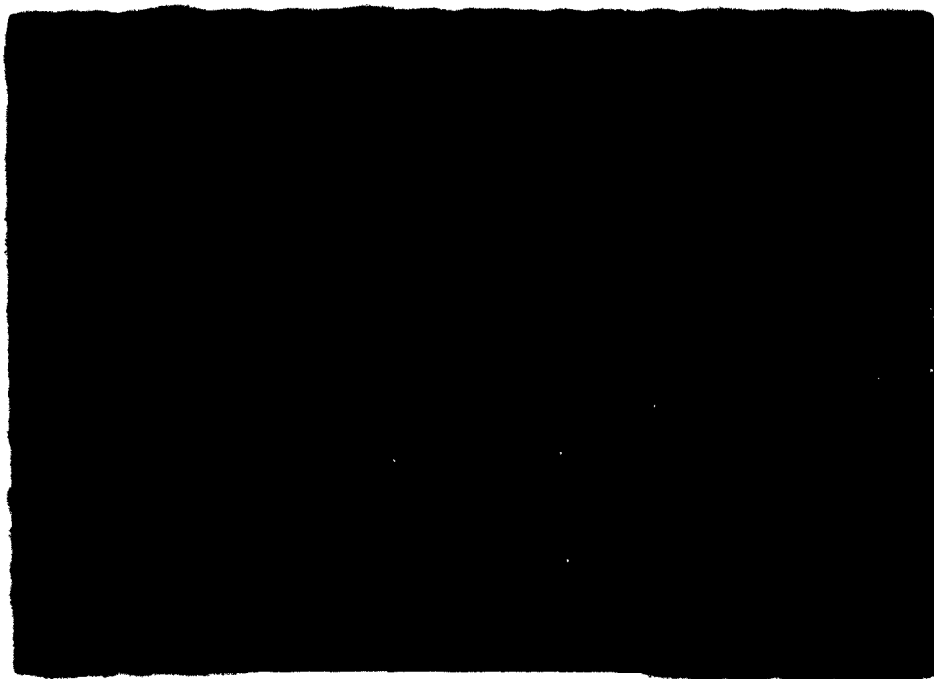


Figure 32. Radar type building, $1\frac{1}{2}$ hr after start of test.

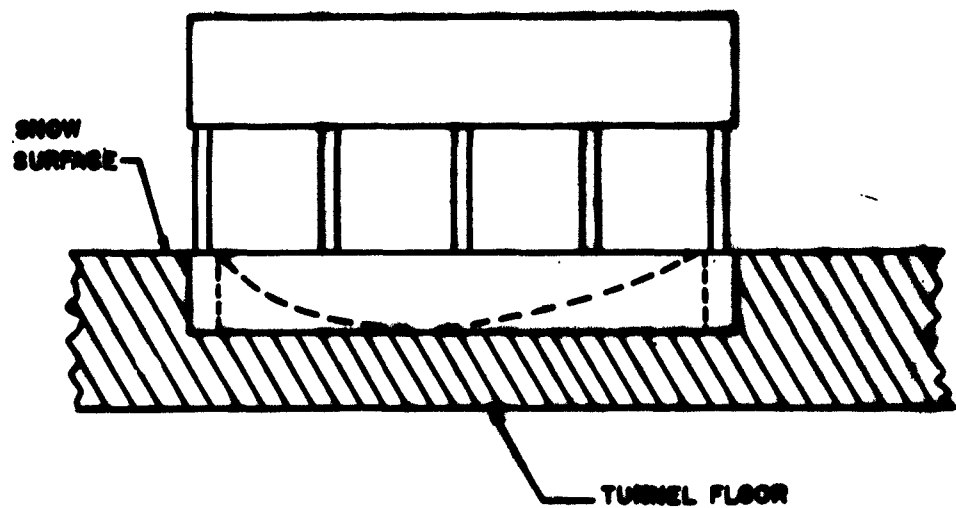


Figure 33. Schematic view of foundation used to support radar type building for test rerun.



Figure 34. Radar type building with special foundation, 2 hr after start of test.



Figure 35. Union Pacific type snow fence inclined 90°, 3 hr after start of test.



Figure 36. Union Pacific type snow fence inclined 60°, 2 hr after start of test.



Figure 37. Model of paper strip fence
tested on the Greenland Ice Cap.



Figure 38. Paper strip fence,
3 hr after start of test.



Figure 39. V-shaped Union Pacific type fence prior to start of test.



Figure 40. Clear area downwind of V-shaped fence, after 2-hr test period.



Figure 41. Models representing 10 ft high fuel tanks, $\frac{1}{2}$ hr after start of test.



Figure 42. Fuel tanks after 3 hr of blowing snow, looking downwind.

REFERENCES

- Bagnold, R. A. (1941) The physics of blown sand and desert dunes. London: Methuen and Co., Ltd., 265p.
- Becker, A. (1944) Natural snow fences along roads, Bautechnik, vol. 22, p. 161-166.
- Dalla Valle, J. M. (1948) Micrometrics, the technology of fine particles. New York: Pitman Publishing Corporation, 555p.
- Diunin, A. K. (1956) "Struktura metelevogo snega i zakonomernosti snegovogo potoka (The structure of blowing snow and the laws governing its flow)", in Voprosy ispol'zovaniia snega, Institut Geografii Akademii Nauk, SSSR, Moscow: Izdatel'stvo Akademii Nauk SSSR, p. 106-119.
- Eshbach, Ovid W. (1936) Handbook of engineering fundamentals. New York: John Wiley and Sons, Inc., 1314p.
- Finney, E. A. (1940) Snow drift control by highway design; result of wind tunnel investigations interpreted, Roads and Streets, vol. 83, no. 3, p. 45-48.
- Gerdel, R. W. (1960) Snow drifting and engineering design, Meteorological Monographs, vol. 4, no. 22, p. 57-64.
- Hallberg, S. (1943) Nagra undersokningar av snoskarmar (Some investigations as to snow fences), Statens Vaginstitut (Stockholm), Meddelande 67, 71p.
- Hamilton, R. A. (1958) The meteorology of North Greenland during the midwinter period, Quarterly Journal of the Royal Meteorological Society, vol. 84, no. 362, p. 355-374.
- Hodgman, Charles D. (1952) Handbook of chemistry and physics, 33rd Edition. Cleveland, Ohio: Chemical Rubber Publishing Company, 2950p.
- Hoerner, S. F. (1958) Fluid dynamic drag. Midland Park, New Jersey: published by the author.
- Nokkentved, C. (1938) Investigation on snow fences, Stads-Og Havneingenioren, vol. 30, no. 8, p. 111-114.
- Perry, John H. (1950) Chemical engineer's handbook. New York: McGraw-Hill Book Company, Inc., 1942p.
- Roots, E. F. and Swithinbank, C. W. M. (1955) Snowdrifts around buildings and stores, Polar Record, vol. 7, no. 50, p. 380-387.
- Schlichting, H. (1955) Boundary layer theory. New York: McGraw-Hill Book Company, Inc., 647p.

<p>AD Accession No.</p> <p>U. S. Army Snow, Ice and Permafrost Research Establishment, Corps of Engineers SCALE MODEL STUDIES ON SNOW DRIFTING - G. H. Strom, G. R. Kelly, E. L. Keitz, and R. F. Weiss</p> <p>Research Report 73, Sept 1962, 50p-illus.-tables. DA Task 8X99-27-001-03, (Contract DA-11-190-ENG-31, New York University College of Engineering) UNCLASSIFIED</p> <p>Scale model tests were conducted to study experimental and theoretical aspects of snow drifting phenomena. Modeling criteria for drifting snow were developed and a number of materials were tested for use as geometrically and physically scaled synthetic snow. Crystalline borax 0.01 cm in diam was found satisfactory for a 1/10 model scale. The feasibility of using scaled materials to simulate drifting snow was demonstrated by the similarity of drift patterns obtained in the wind tunnel tests and those observed around full-scale structures on the Greenland Ice Cap. Further, several years of Arctic snow drift can be simulated in the wind tunnel in a matter of hours. Qualitative analyses are offered of drift accumulation characteristics around various scale model structures. The following experimental results were obtained.</p>	<p>UNCLASSIFIED</p> <p>1. Snow drifts 2. Models (snow) I. Strom, Gordon H. II. Kelly, George R. III. Keitz, Edwin L. IV. Weiss, Robert F. V. U. S. Army Snow, Ice and Permafrost Research Establishment VI. New York University College of Engineering VII. Contract DA-11-190-ENG-31</p>	<p>AD Accession No.</p> <p>U. S. Army Snow, Ice and Permafrost Research Establishment, Corps of Engineers SCALE MODEL STUDIES ON SNOW DRIFTING - G. H. Strom, G. R. Kelly, E. L. Keitz, and R. F. Weiss</p> <p>Research Report 73, Sept 1962, 50p-illus.-tables. DA Task 8X99-27-001-03, (Contract DA-11-190-ENG-31, New York University College of Engineering) UNCLASSIFIED</p> <p>Scale model tests were conducted to study experimental and theoretical aspects of snow drifting phenomena. Modeling criteria for drifting snow were developed and a number of materials were tested for use as geometrically and physically scaled synthetic snow. Crystalline borax 0.01 cm in diam was found satisfactory for a 1/10 model scale. The feasibility of using scaled materials to simulate drifting snow was demonstrated by the similarity of drift patterns obtained in the wind tunnel tests and those observed around full-scale structures on the Greenland Ice Cap. Further, several years of Arctic snow drift can be simulated in the wind tunnel in a matter of hours. Qualitative analyses are offered of drift accumulation characteristics around various scale model structures. The following experimental results were obtained.</p>	<p>UNCLASSIFIED</p> <p>1. Snow drifts 2. Models (snow) I. Strom, Gordon H. II. Kelly, George R. III. Keitz, Edwin L. IV. Weiss, Robert F. V. U. S. Army Snow, Ice and Permafrost Research Establishment VI. New York University College of Engineering VII. Contract DA-11-190-ENG-31</p>
<p>AD Accession No.</p> <p>U. S. Army Snow, Ice and Permafrost Research Establishment, Corps of Engineers SCALE MODEL STUDIES ON SNOW DRIFTING - G. H. Strom, G. R. Kelly, E. L. Keitz, and R. F. Weiss</p> <p>Research Report 73, Sept 1962, 50p-illus.-tables. DA Task 8X99-27-001-03, (Contract DA-11-190-ENG-31, New York University College of Engineering) UNCLASSIFIED</p> <p>Scale model tests were conducted to study experimental and theoretical aspects of snow drifting phenomena. Modeling criteria for drifting snow were developed and a number of materials were tested for use as geometrically and physically scaled synthetic snow. Crystalline borax 0.01 cm in diam was found satisfactory for a 1/10 model scale. The feasibility of using scaled materials to simulate drifting snow was demonstrated by the similarity of drift patterns obtained in the wind tunnel tests and those observed around full-scale structures on the Greenland Ice Cap. Further, several years of Arctic snow drift can be simulated in the wind tunnel in a matter of hours. Qualitative analyses are offered of drift accumulation characteristics around various scale model structures. The following experimental results were obtained.</p>	<p>UNCLASSIFIED</p> <p>1. Snow drifts 2. Models (snow) I. Strom, Gordon H. II. Kelly, George R. III. Keitz, Edwin L. IV. Weiss, Robert F. V. U. S. Army Snow, Ice and Permafrost Research Establishment VI. New York University College of Engineering VII. Contract DA-11-190-ENG-31</p>	<p>AD Accession No.</p> <p>U. S. Army Snow, Ice and Permafrost Research Establishment, Corps of Engineers SCALE MODEL STUDIES ON SNOW DRIFTING - G. H. Strom, G. R. Kelly, E. L. Keitz, and R. F. Weiss</p> <p>Research Report 73, Sept 1962, 50p-illus.-tables. DA Task 8X99-27-001-03, (Contract DA-11-190-ENG-31, New York University College of Engineering) UNCLASSIFIED</p> <p>Scale model tests were conducted to study experimental and theoretical aspects of snow drifting phenomena. Modeling criteria for drifting snow were developed and a number of materials were tested for use as geometrically and physically scaled synthetic snow. Crystalline borax 0.01 cm in diam was found satisfactory for a 1/10 model scale. The feasibility of using scaled materials to simulate drifting snow was demonstrated by the similarity of drift patterns obtained in the wind tunnel tests and those observed around full-scale structures on the Greenland Ice Cap. Further, several years of Arctic snow drift can be simulated in the wind tunnel in a matter of hours. Qualitative analyses are offered of drift accumulation characteristics around various scale model structures. The following experimental results were obtained.</p>	<p>UNCLASSIFIED</p> <p>1. Snow drifts 2. Models (snow) I. Strom, Gordon H. II. Kelly, George R. III. Keitz, Edwin L. IV. Weiss, Robert F. V. U. S. Army Snow, Ice and Permafrost Research Establishment VI. New York University College of Engineering VII. Contract DA-11-190-ENG-31</p>

<p>(1) Close spacing of buildings will result in coalescence of drifts. (2) If rectangular buildings must be grouped together, they should be erected with their long axis parallel to the dominant wind direction. (3) Erosion of the snow surface may occur beneath buildings erected on columns. (4) V-shaped snow fences produce a clear area downwind for a distance of approximately 25 times the height of the fence.</p>		<p>(1) Close spacing of buildings will result in coalescence of drifts. (2) If rectangular buildings must be grouped together, they should be erected with their long axis parallel to the dominant wind direction. (3) Erosion of the snow surface may occur beneath buildings erected on columns. (4) V-shaped snow fences produce a clear area downwind for a distance of approximately 25 times the height of the fence.</p>
<p>(1) Close spacing of buildings will result in coalescence of drifts. (2) If rectangular buildings must be grouped together, they should be erected with their long axis parallel to the dominant wind direction. (3) Erosion of the snow surface may occur beneath buildings erected on columns. (4) V-shaped snow fences produce a clear area downwind for a distance of approximately 25 times the height of the fence.</p>		<p>(1) Close spacing of buildings will result in coalescence of drifts. (2) If rectangular buildings must be grouped together, they should be erected with their long axis parallel to the dominant wind direction. (3) Erosion of the snow surface may occur beneath buildings erected on columns. (4) V-shaped snow fences produce a clear area downwind for a distance of approximately 25 times the height of the fence.</p>